Journal of Biomedical Optics

BiomedicalOptics.SPIEDigitalLibrary.org

Review of optical breast imaging and spectroscopy

Dirk Grosenick
Herbert Rinneberg
Rinaldo Cubeddu
Paola Taroni

SPIE.

Dirk Grosenick, Herbert Rinneberg, Rinaldo Cubeddu, Paola Taroni, "Review of optical breast imaging and spectroscopy," *J. Biomed. Opt.* **21**(9), 091311 (2016), doi: 10.1117/1.JBO.21.9.091311.

Journal of Biomedical Optics 21(9), 091311 (September 2016)

REVIEW

Review of optical breast imaging and spectroscopy

Dirk Grosenick,[a,*] Herbert Rinneberg,[a] Rinaldo Cubeddu,[b] and Paola Taroni[b]
[a]Physikalisch-Technische Bundesanstalt, Abbestrasse 2-12, 10587 Berlin, Germany
[b]Politecnico di Milano, Dipartimento di Fisica, Piazza Leonardo da Vinci 32, 20133 Milano, Italy

Abstract. Diffuse optical imaging and spectroscopy of the female breast is an area of active research. We review the present status of this field and discuss the broad range of methodologies and applications. Starting with a brief overview on breast physiology, the remodeling of vasculature and extracellular matrix caused by solid tumors is highlighted that is relevant for contrast in optical imaging. Then, the various instrumental techniques and the related methods of data analysis and image generation are described and compared including multimodality instrumentation, fluorescence mammography, broadband spectroscopy, and diffuse correlation spectroscopy. We review the clinical results on functional properties of malignant and benign breast lesions compared to host tissue and discuss the various methods to improve contrast between healthy and diseased tissue, such as enhanced spectroscopic information, dynamic variations of functional properties, pharmacokinetics of extrinsic contrast agents, including the enhanced permeability and retention effect. We discuss research on monitoring neoadjuvant chemotherapy and on breast cancer risk assessment as potential clinical applications of optical breast imaging and spectroscopy. Moreover, we consider new experimental approaches, such as photoacoustic imaging and long-wavelength tissue spectroscopy. [DOI: 10.1117/1.JBO.21.9.091311]

Keywords: breast cancer; optical mammography; multimodality techniques; near-infrared spectroscopy; diffuse correlation spectroscopy.

Paper 160029SSVR received Jan. 15, 2016; accepted for publication Jun. 13, 2016; published online Jul. 11, 2016.

1 Introduction

Breast cancer is the most common cancer of women and the second leading cause of death after cardiovascular disease in many countries. About one in eight women will be diagnosed with this disease during their lifetimes in the United States and in European countries.[1,2] Early diagnosis of breast cancer is essential to ensure a high chance of survival for the affected women. Therefore, an important task is to provide diagnostic tools with high sensitivity for early detection of breast cancer and high specificity to avoid false positive results.

Today's first line imaging modality is x-ray mammography. Several countries have implemented mammography screening programs with the aim of early detection of the disease. However, the sensitivity of conventional x-ray mammography is only about 75%.[3] For radiographic dense breast tissue, which is more common in younger women, the sensitivity can even drop below 50%.[3] Considering that frequent x-ray exposure can promote the development of cancer on a long time scale mammographic screening is often discussed controversially. Magnetic resonance imaging (MRI) of the breast offers higher sensitivity, yet its specificity is rather poor.[4,5] Moreover, it is characterized by high costs and long examination times prohibiting screening. Currently, this method is in use as an additional modality for selected women with suspicious lesions. Similarly, breast ultrasound is often used as a supplementary tool. Its results are strongly dependent on the examiner's interpretation. In general, biopsies, which are at the end of today's breast cancer detection clinical work flow, show a large number of false-positive cases for the established imaging modalities.[6,7]

Besides the problem of detection and differentiation, tools are needed to support or monitor the therapy of breast cancer. A main part of treatment is the surgical removal of the cancerous tissue. The today's preferred way of breast-conserving surgery requires methods to safely detect tumor margins. Furthermore, the treatment of large cancers often starts with neoadjuvant chemotherapy (NAC) to shrink the size of the tumor before surgery. This shrinking process needs to be monitored by a suited method. Currently, MRI is most often used to this end.[8] However, a less costly method not requiring application of contrast agents is highly desirable, in particular for frequently repeated use.

During the last 15 years, optical imaging of the breast has been investigated by many research groups as well as by companies in order to develop tools that could yield considerable contributions to the mentioned steps in breast cancer management, i.e., to the detection of breast cancer, to its differentiation, and to monitor its treatment. Starting from the idea to detect breast cancer by near-infrared spectroscopy from contrast in hemoglobin concentration and blood oxygen saturation, the potential of optical imaging of the breast can now be realistically assessed due to the large amount of data obtained from clinical studies. However, definite conclusions are still difficult to draw, as clinical studies were typically conducted with different instruments, different methods of data analysis, and various clinical protocols, making results often difficult to compare. Although the original aim of developing a new tool for screening that could compete with x-ray mammography could not be reached so far, optical breast imaging has found potentially new areas of application, such as monitoring of neoadjuvant therapy progress and determination of risk populations for breast cancer development. Furthermore, the application of contrast agents seems to be a promising way for breast cancer imaging.

*Address all correspondence to: Dirk Grosenick, E-mail: dirk.grosenick@ptb.de

In this paper, we review the development of optical breast imaging by near-infrared spectroscopy, including contrast agent enhanced methodology. We start with a discussion of breast physiology and with the main features of breast imaging instrumentation and data analysis approaches. Then, we consider the available results on optical properties of the healthy breast and of malignant and benign lesions and the various methods to improve the contrast between healthy and diseased tissue. We review research on monitoring neodjuvant chemotherapy and on risk assessment as potential applications. And finally, we consider new experimental approaches, such as photoacoustic imaging (PI) and long wavelength broadband spectroscopy.

2 Fundamentals of Optical Breast Imaging

2.1 *Biomedical Background*

2.1.1 *Overall structure and composition of normal breast tissue*

Optical mammography and diffuse optical spectroscopy of the human breast probe the absorption, scattering, and fluorescence properties of various components of healthy and diseased breast tissue. The human female breast consists mainly of glandular, adipose, and connective tissue, together with blood and lymphatic vessels, and it contains several simple mammary glands (lobes), each draining through a separate lactiferous duct. The lobes branch into several lobules consisting of intralobular ducts separated by rather loose (intralobular) connective tissue, containing microvasculature and small lymphatic channels. Each intralobular ductal tree terminates in a cluster of alveoli that will differentiate to produce milk on exposure to lactogenic hormones. The intralobular connective tissue and ductal network are surrounded by the interstitial connective tissue, being dense, less cellular, containing variable proportions of adipose tissue and extracellular matrix (ECM), and representing over 80% of the human breast volume.[9]

Besides blood and lymphatic vessels, the connective tissue (stroma) consists of various stromal cells and the ECM (see Fig. 1), providing a scaffold for stromal cells (e.g., fibroblasts, adipocytes, cells of the immune system, e.g., lymphocytes, macrophages).[10] The ECM is composed of water, proteins, and polysaccharides.[11] Proteoglycans (PGs) and fibrous proteins (e.g., collagens, fibronectin, elastins) are the two main classes of macromolecules of the ECM, forming an intricate interlocking mesh.[11] The polysaccharides glycosaminoglycans (GAGs) are usually attached to ECM proteins to form PGs. PGs fill the majority of the extracellular interstitial space within the tissue in the form of a hydrated gel.[11] PGs have a net negative charge that attracts sodium ions and in consequence water, keeping the ECM and resident cells hydrated. Unlike other GAGs, the polysaccharide hyaluronic acid (or "hyaluronan") contained in the ECM is not bound to matrix proteins. Hyaluronic acid in the extracellular space confers upon tissues the ability to resist compression providing a counteracting swelling force by absorbing significant amounts of water. Collagens constitute the main structural element of the ECM and, together with other fibrous proteins, provide mechanical strength and elasticity to the tissue.[11] Nonactivated tissue fibroblasts secrete various ECM proteins (collagens and elastins) and PGs including hyaluronic acid.[11] The ECM, containing various peptides, e.g., growth factors and enzymes, is being constantly remodeled for tissue homeostasis. Such remodeling is regulated by a careful balance between intracellular matrix synthesis, secretion, modification, e.g., crosslinking of collagens by lysyl oxidases (LOX) and enzymatic degradation, e.g., by matrix metalloproteases (MMPs).[12] The ECM not only represents scaffolding for the stromal cells but also conveys biochemical and biophysical signals to cells.

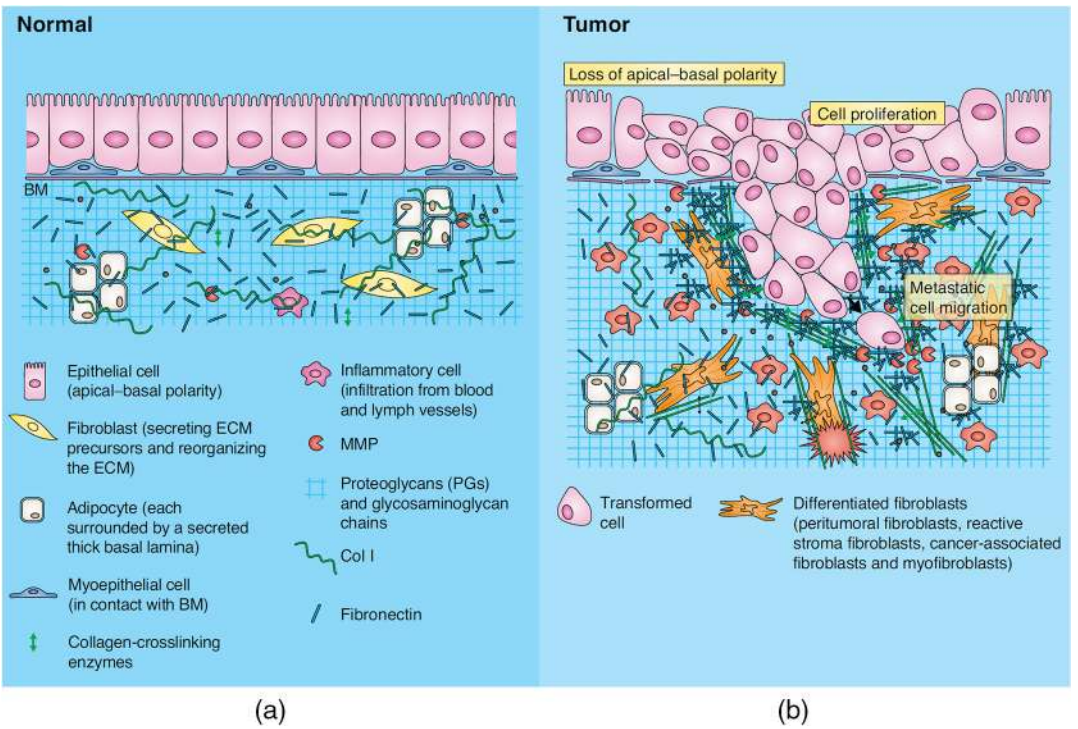

Fig. 1 Structure and function of ECM in (a) normal and (b) tumorous glandular epithelial tissue (e.g., breast). (Reprinted with permission from Frantz et al.[11])

2.1.2 *Abnormal vasculature and lymphatics of solid tumors*

Solid tumors are not simply a collection of neoplastic cells but have been considered to be abnormal organs, with abnormal vasculature and lymphatics, abnormal ECM, and populations of stromal cells differing from normal host tissue.[10,13] The vasculature of solid tumors differs distinctly from that of surrounding host tissue. Vasculature in normal tissue is arranged in a hierarchy of arteries–arterioles–capillaries–venules and veins, and grows under strict control of intervessel distances to ensure sufficient supply of oxygen and nutrients to cells by diffusion after extravasation, whereas tumor vasculature develops in a chaotic manner without such control, leading to chaotic interconnectivity of vessel segments and spatial vascular heterogeneity. In solid tumors, necrotic regions and regions of low microvessel density may occur, whereas tumor blood vessels are more abundant at the tumor–host interface.[14]

Tumors may co-opt existing host vasculature for supply of oxygen and nutrients,[15,16] yet new vasculature must generally develop for tumors to grow beyond 1 to 2 mm^3 in size.[17] New blood vessels may be grown from existing vasculature by angiogenic sprouting, followed by growth of sprouts and their fusion with existing vessels to form new perfused blood vessels (neoangiogenesis).[16,18,19] Vascular sprouting is initiated by vascular epithelial growth factor (VEGF), which is secreted by, e.g., hypoxic tumor cells. VEGF works in concert with other growth factors, e.g., angiopoietin-1 (ANG-1) and angiopoietin-2 (ANG-2). ANG-1 is involved in vessel maturation.[19] On the other hand, ANG-2 disrupts the connections between the endothelium and perivascular cells and thus promotes cell death and vascular regression. Yet, in conjunction with VEGF, ANG-2 promotes neovascularization. By destabilizing existing vessels, ANG-2 allows for the formation of sprouts, thus contributing to neoangiogenesis, provided VEGF is present at sufficient concentration.[16,19,20] In solid tumors, guidance proteins (EphB4) have been shown to act as negative regulators of blood vessel branching and vascular network formation, switching the vascularization program from sprouting angiogenesis to circumferential vessel growth.[21] Neovascularization in solid tumors involves many complex processes of different origin and molecular pathways,[22] whereas processes of angiogenesis are strictly controlled under physiological conditions; this is no longer true in solid tumors, and tumor vessels turn out to be immature, fragile, tortuous, dilated, with uneven diameters, and known to form (large diameter) arteriovenous shunts. Often, it is even difficult to distinguish arterioles from venules in solid tumors, i.e., the classification of tumor vessels as arterioles, capillaries, and venules is no longer adequate.[13,14,18,23]

Tumor cells that are considerably farther apart from nearby capillaries than the diffusion limit of oxygen (typically 100 to 200 μm) suffer from chronic (diffusion limited) hypoxia. Furthermore, the structurally abnormal tumor vasculature results in spatially and temporally heterogeneous blood flow, affecting tissue oxygenation (acute or perfusion-limited hypoxia).[24] From intravital dorsal window microscopy on tumor models, it is known that blood flow through tumor capillaries is frequently sluggish and at times may even be stationary and reverse direction.[23] It follows that blood flow through tumors may not follow a constant unidirectional path. In addition, red blood cell (RBC) flux varies greatly among tumor vessels; many tumor vessels do not carry RBCs but contain plasma only.[24] Solid stress, caused by tumor cell proliferation and increased ECM deposition in tumors, may compress or block existing vasculature, impeding blood flow and, hence, the supply of oxygen and nutrients.[9,25–27]

Tumor hypoxia is associated with poor prognosis, because it causes resistance to standard therapies and promotes more aggressive tumor phenotypes.[28] Hypoxic tumor cells are known to be resistant to ionizing radiation, since oxygen is needed to stabilize radiation-induced DNA defects and, in addition, are considered to be resistant to some anticancer drugs.[28,29] Furthermore, T-cells are dependent on normal oxygen levels for migration in tumor tissue, suggesting that hypoxia indirectly regulates antitumor immunity by restricting T-cell access.[10]

Tumor vessels may exhibit high permeability to macromolecules, e.g., to plasma proteins such as albumin.[18,30] Generally, lymphatic drainage is impaired in tumors, since lymphatic vessels are sparse or even absent. Because of the leakiness of tumor vasculature, interstitial fluid pressure rises from, e.g., 0 mmHg in normal breast tissue up to 30 mmHg in breast cancers or even higher,[13] impeding extravascular fluid flow and transport of extravasated macromolecules including chemotherapeutics, causing the so-called enhanced permeability and retention (EPR) effect.[30,31] Macromolecules administered intravenously or small molecules, e.g., drugs that associate with plasma proteins, may not extravasate from normal vasculature, yet may leak into the interstitial matrix from tumor vasculature due to its enhanced permeability and stay there because of impaired lymphatic drainage.

2.1.3 *Abnormal extracellular matrix of solid tumors*

It has long been known that tumor-derived ECM is biochemically distinct in its composition compared with normal ECM (Fig. 1).[12] Breast cancer progression is associated with changes in ECM composition, with inflammatory cell infiltration, and differentiation of fibroblasts.[9] Tumor-derived ECM differs from that of the host tissue, owing to the disruption of the balance between ECM synthesis and secretion and owing to alterations in the normal levels of matrix-remodeling enzymes, such as MMP and LOX.[12] The ECM remodeling observed in tumors includes increased deposition of collagen, fibronectin, PGs, substantial MMP-dependent cleavage, and increased levels of LOX-dependent matrix crosslinking. There is evidence for an increased deposition of ECM in hypoxic tumor regions.[32] Differentiated fibroblasts (e.g., myofibroblasts) deposit large amounts of ECM proteins.[11] The expression of MMPs is often highly upregulated in solid tumors with MMPs produced by myofibroblasts and tumor cells.[11] ECM deposition and leukocyte infiltration are often very pronounced at the tumor-stroma border.[10] The majority of increased tumor and adjacent tissue stiffness occur as a result of increased ECM deposition.[12] Furthermore, increased LOX activity results in increased ECM stiffness.[12] As illustrated in Fig. 2, the expanding tumor mass exerts compressive stress (tissue solid stress) on the surrounding tissue, on the ECM, on intratumoral vasculature and lymphatics.[9,25] NIR imaging is directly affected by the modifications of the ECM occurring in tumors, resulting in changes of the tissue absorption spectrum. For example, additional deposition of collagen increases long-wavelength (1060 nm) absorption, while tissue solid stress on tumor vasculature may affect blood flow, resulting in changes of oxyhemoglobin concentration and corresponding modifications of the absorption spectrum.

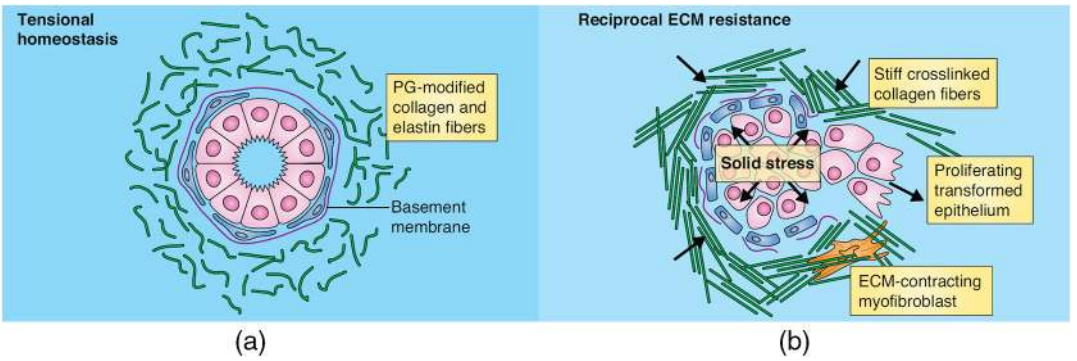

Fig. 2 Extrinsic and intrinsic forces on (a) normal and (b) tumorous glandular epithelial tissue (e.g., breast). (Reprinted with permission from Frantz et al.[11])

2.1.4 *Expected solid tumor-host optical contrast*

Within the optical window, extending from about 635 up to 1060 nm breast tissue optical spectroscopy yields the absorption coefficient $\mu_a(\lambda)$ and reduced scattering coefficient $\mu_s'(\lambda)$ of the host and tumor tissue. From average absorption coefficients $\mu_a(\lambda)$, concentrations of the main tissue constituents deoxyhemoglobin (HbR), oxyhemoglobin (HbO_2), and thus, total hemoglobin $HbT = HbR + HbO_2$, water, lipids, and collagen can be inferred using Beer's law. Total tissue hemoglobin concentration, HbT, can be converted to vascular volume fraction rBV (vascular volume density) according to $HbT = MCHC \times H \times rBV$ where MCHC is the mean corpuscular hemoglobin concentration and hematocrit H is assumed to be homogeneous within the vasculature. Because of angiogenesis and circumferential vessel growth occurring in tumors, one expects higher vascular volume fraction and thus higher total tissue hemoglobin concentrations in tumorous compared to host tissue $HbT_{(T)} > HbT_{(N)}$ (see Sec. 4.1). Tissue blood oxygen saturation, defined as $StO_2 = HbO_2/HbT$, depends not only on vascular structure but also on transvascular oxygen loss, i.e., on tissue metabolic rate of oxygen consumption and on vascular oxygen supply, i.e., on perfusion. From tumor biology, the concentration of collagen is expected to be higher in breast tumors compared to surrounding host tissue. Likewise, because of the additional deposition of the ECM in tumors and the hydrophilic nature of PGs contained, higher water content in breast tumors is predicted.

Apart from absorption, light scattering in tissue provides information on tissue structure and composition. Light scattering in tissue is dominated by Mie scattering and, therefore, probes density and size of biological cells; however, scattering by other tissue structures, such as collagen fibrils, cannot be excluded. Because of tumor cell proliferation and infiltration of various cells (e.g., inflammatory cells, differentiated fibroblasts) into the tumor stroma, cell density and, hence, the reduced scattering coefficient μ_s' are expected to be increased in tumors compared to their surrounding host tissue. Furthermore, formation of large modified collagen bundles likely affects photon scattering (see Fig. 2). As discussed in Sec. 4.1, most of these predictions are borne out by experimental data.

2.2 *Historical Development of Optical Breast Imaging*

First attempts to see suspicious lesions in the female breast using visible light were reported by Cutler in 1929.[33,34] The breast was transilluminated by holding a small size powerful lamp against the lower surface of the breast and by observing shadows of the light on the upper breast side by eye that arose from high-absorbing tissue structures. In the 1970s and 1980s, transillumination imaging of the breast was further developed by using improved light sources in combination with light detection by sensitive films or video cameras.[35–39] However, several clinical studies showed that sensitivity and specificity of the so-called lightscanning or "diaphanography" method were low in comparison to x-ray mammography.[40–43] The lightscanning approach was very simple to apply, but it had major intrinsic disadvantages, including the absence of discrimination between scattering and absorption of the tissue and the limited exploitation of spectral information.

New efforts in optical breast imaging started in the 1990s. At that time, mathematical models of light propagation in tissue became available that permitted separation of the scattering and the absorption properties of the tissue. In this way, absorption properties could be exploited by the methods of near-infrared spectroscopy to determine the composition of the tissue, i.e., to measure the concentrations of the main tissue absorbers including blood oxygen saturation. Basic concepts of optical breast imaging developed at this time are valid until today.

2.3 *Classification of Optical Breast Imagers*

Normally, optical images of the breast are obtained by switching through a sufficient number of point-like light sources realized by illuminated optical fibers and, for each source, detecting the light at one or several suited detector positions. The instruments for optical breast imaging and spectroscopy can be classified with respect to the temporal profile of the laser radiation employed and according to their measurement geometry. Furthermore, a few instruments have been designed to detect fluorescence arising from an exogenous contrast agent. The three well-known groups of instruments are time-domain, frequency-domain, and continuous-wave (CW) systems. Briefly, time-domain systems measure the broadening of short (picosecond) laser pulses after propagation through the tissue. Absorption coefficients μ_a and reduced scattering coefficients μ_s' of the tissue can be derived from the analysis of the detected pulse shape using an appropriate model of photon propagation. These coefficients characterize the tissue volume sampled by photons depending on the particular source–detector combination. For source–detector separations of a few centimeters, the width of the broadened pulses amounts typically to a few nanoseconds. A well-suited technique for the detection of these pulses is time-correlated single-photon counting. In the past, hardware

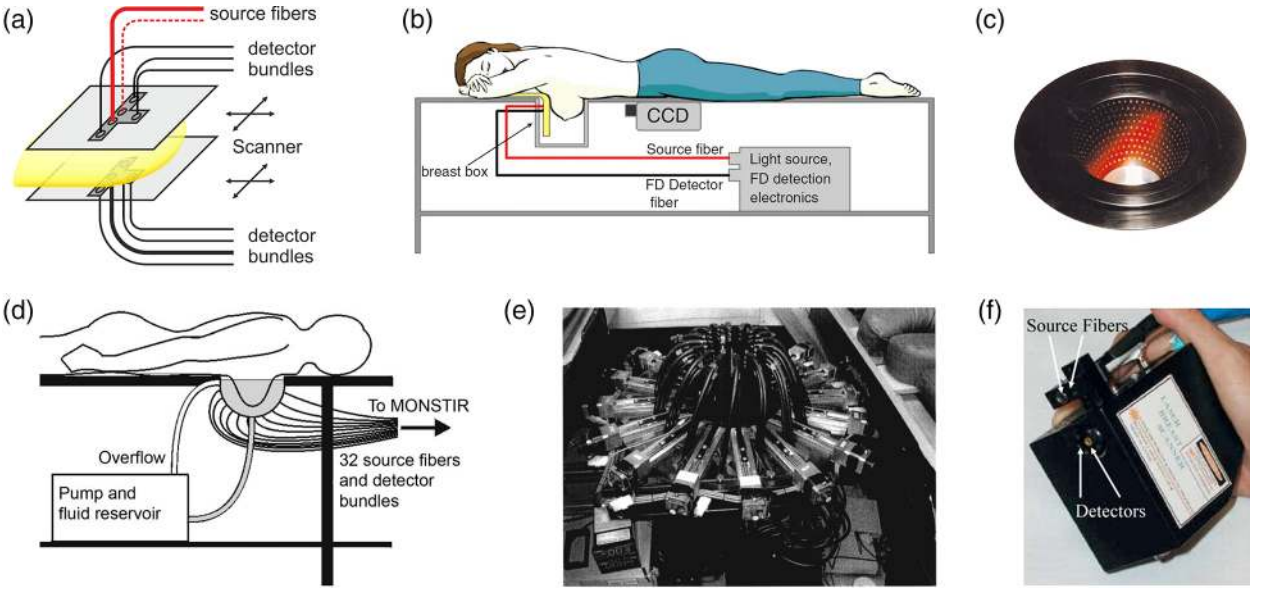

Fig. 3 Examples of measurement geometries: (a) parallel-plate geometry with moving source fiber and few detector fibers in transmission and reflection,[46] (b) parallel-plate geometry with fixed source and detector fibers (left) and CCD camera detection (right) (reprinted with permission from Choe et al.[47]), (c) freely pending breast geometry with 255 source and 255 detector fibers (© 1999 IEEE. Reprinted with permission from Colak et al.[48]), (d) freely pending breast with 32 sources and 32 detectors (reprinted with permission of Optical Society of America from Enfield et al.[49]), (e) circular arrangement of 48 fibers in three rings with 16 translation stages to bring the fibers in contact with the tissue (reprinted with permission from Pogue et al.[50]), and (f) handheld probe (reprinted with permission from O'Sullivan et al.[51]).

for time-domain systems was expensive. However, it is now becoming possible to perform time-resolved data acquisition with more cost-competitive instrumentation.

Frequency-domain systems use intensity-modulated laser radiation and measure its demodulation and phase shift after passing through tissue. In principle, it is sufficient to perform such measurements at one modulation frequency to separate the absorption and the scattering coefficient of the sampled tissue volume. Typically, a modulation frequency of about 100 MHz is chosen. Frequency-domain measurements correspond to investigating the Fourier spectrum of time-domain measurements at one frequency. By employing several modulation frequencies up to at least 1 GHz, the information content of frequency domain measurements increases and becomes comparable to that of typical time-domain investigations.

CW systems use continuously emitting lasers or light-emitting diodes at several near-infrared wavelengths, or broadband light sources. The instruments detect the attenuation of the transmitted light. More specifically, the CW technique yields the attenuation coefficient $\kappa = \sqrt{\mu_a/D}$, which is a combination of the absorption coefficient μ_a and the diffusion coefficient $D = 1/3\mu_s'$. To obtain absolute values of the absorption coefficients, prior knowledge on the reduced scattering coefficient is required, e.g., from additional investigations with the frequency-domain or time-domain technique or by using representative values from literature. However, because light scattering dominates over absorption within the optical window, the latter approach may lead to systematic errors. Alternatively, it is possible to assess both absorption and scattering properties by performing CW measurements at more than one source–detector separation, which has been used, e.g., to obtain properties of small (almost homogeneous) tissue regions.[44] Generally, it is also possible to exploit spectral features for the separation of absorption and scattering by using specifically selected optical wavelengths.[45] The main advantage of the CW approach is that light sources and detectors are comparably cheap. Therefore, such systems can be equipped with a large number of source and detector positions at low costs.

The geometry for optical breast imaging can be divided into three main groups (Fig. 3). In one approach, the breast is compressed between two parallel plates. This geometry is very close to the concept of x-ray mammography. It offers a simple way to compare an optical transillumination image with a corresponding x-ray mammogram. A second approach consists of investigating the freely pending breast with the woman being in prone position. This geometry has high similarity with MRI of the breast. The third basic approach is the use of a handheld probe that can be positioned at selected locations of the breast or moved over its surface similar to a breast ultrasound detector. It is obvious that these three geometries offer the possibility for combining optical imaging with x-ray, MR, or US breast imaging, which was pursued by several groups, mainly to gain prior information on spatial tissue composition, lesion size, and position when analyzing their optical and functional properties.

3 State-of-the-Art Instrumentation and Data Analysis

3.1 *Overview on Optical Breast Imagers*

Figure 3 shows several examples of the measurement geometry and the source–detector arrangements that were realized in instrumentation for clinical studies on optical breast imaging.

A simple way to realize the compression geometry is the application of two transparent plates with variable distance [Fig. 3(a)]. Optical transillumination images of the breast can

be obtained by moving a source fiber on one side and a detector fiber on the other side in tandem. Such systems have first been developed by the German companies Siemens and Carl Zeiss.[52,53] Both systems were equipped with frequency-domain instrumentation. Later, the Physikalisch-Technische Bundesanstalt[54] and the Politecnico di Milano[55] used this geometry to build-up the first time-domain scanning optical mammographs. At Tufts University, the compression geometry has been employed more recently in a hybrid instrument combining frequency-domain measurements at a few near-infrared wavelengths with broadband CW spectroscopy[56] and in an instrument using solely CW radiation.[57] With a scanning step size of a few millimeters or even less, typically, more than 1000 source–detector combinations (scan positions) are sampled.

As an example for the parallel plate geometry, the schematic in Fig. 3(a) shows the latest source–detector fiber arrangement of the PTB instrument with several detection fibers in transmission and also detection fibers in reflection.[46] The various fibers in transmission permit the detection of transillumination images at the implemented optical wavelengths under different projection angles, which can be exploited to reconstruct three-dimensional (3-D) images of the tissue.[46,58] The additional detection fibers in reflection can be used to improve the 3-D resolution close to the surface, as shown in phantom experiments.[59] However, with a transparent plate, only distances from the source fiber below, typically, 1 cm can be exploited due to multiple reflections occurring within the plate. Figure 3(a) shows a second source fiber (dashed line), that was added to the PTB optical mammograph for fluorescence measurements. The tandem scanner concept with several offset fibers in transmission is also employed in the latest version of the CW optical mammograph developed at Tufts University.[57]

Figure 3(b) illustrates the parallel-plate instrument developed at University of Pennsylvania. This hybrid CW-frequency domain device uses the compression geometry with a source–detector arrangement optimized for tomographic reconstruction. The patient is in the prone position with both breasts hanging in a tank filled with a scattering fluid. The opaque compression plate on the left-hand side is equipped with 45 fixed source fibers and 9 fixed detector fibers. The frequency-domain approach is employed to measure the diffusely reflected light at four wavelengths. The CCD camera on the right-hand side in Fig. 3(b) is used to measure the diffuse transmittance of the breast by the CW approach at up to six wavelengths.[47] This device was extended with an option for fluorescence measurements using indocyanine green (ICG) as contrast agent.[60] There were also two time-domain devices developed that use the parallel-plate geometry with matching fluid chamber, the commercial system Softscan of Advanced Research Technologies (ART) Inc., Montreal,[61] and a laboratory prototype at the Physikalisch-Technische Bundesanstalt Berlin.[62] Both these devices employed the concept of scanning source and detector fibers along transparent plates. Depth resolution was achieved by either offset detection channels in transmission similar to Fig. 3(a) or by two CCD cameras similar to Fig. 3(b). The PTB device was also capable of performing fluorescence investigations. The company DOBI Medical International Inc. developed the parallel-plate device ComfortScan for imaging pressure-induced changes in the blood oxygen saturation of tumors. This instrument uses flat-field illumination at 640 nm by LEDs and CCD camera detection of the transmitted light.[63]

Figures 3(c) and 3(d) show examples of devices with a cup-like chamber for investigations of the freely pending breast. The cup in Fig. 3(c) belongs to the CW instrument built by Philips, Eindhoven. In this device, a total of 255 source fibers and 255 interleaved detection fibers were used to reconstruct the tissue attenuation coefficient at three optical wavelengths.[48] The same geometry was used in the fluorescence instrument developed about 10 years later.[64] The time-domain instrument in Fig. 3(d) was built at the University College London. It is equipped with 32 source fibers and 32 detection fiber bundles and provides 3-D images of the absorption and scattering properties at two wavelengths.[49] Both these devices with cup geometry use a scattering fluid to get high quality optical coupling and to work with a well-defined geometry for reconstruction of the optical properties. In order to account for breasts of different sizes, cups with different diameters can be used.

At Dartmouth College, a frequency-domain instrument with six optical wavelengths was developed for investigations on the freely pending breast that does not need a scattering fluid [see Fig. 3(e)]. Here, 48 fibers, which are arranged on three rings, are brought in contact with the tissue under slight pressure.[50] In a newer version, the wavelength range of the device was extended up to 948 nm employing CW lasers.[65] The breast imager developed by NIRx Technologies uses the same principle of pressure-induced optode contact. From these four wavelengths, the CW instrument permits simultaneous investigations on both breasts of the patient. It has been designed for dynamic investigations to record the physiological response of the breast tissue to specific interventions, such as the Valsalva maneuver or to dynamically observe the effect of a contrast agent bolus.[66,67] The company, Imaging Diagnostics Systems, Inc., Fort Lauderdale, followed the principle of CT scanners and developed devices in which the freely pending breast of the patient in prone position is scanned by moving a laser beam and a detector array circularly around the tissue. By changing vertical positions, contiguous slices of the breast are acquired at one optical wavelength.[68,69] Hereby, the detectors are not in contact with tissue. An extended version of these devices was prepared for fluorescence investigations.

Detection limits of diffuse optical tomography systems were investigated theoretically and numerically.[70,71] The method consists of analyzing raw numerical phantom data by means of a chi-square test, obtained from forward simulations together with a realistic noise model, derived from the system hardware. Both parallel-plate and cup geometries were compared with respect to detection limits of heterogeneities at various positions within the tomographic volume investigated. In cup geometry, low detection sensitivity was obtained at the upper center of the cup [cf., Figs. 3(c) and 3(d)], i.e., close to the chest wall, where the tissue is exclusively sampled by source–detector combinations with large separations. In slab geometry, detection sensitivity shows only small variations between the outer and the inner tissue regions, since the breast is sampled with constant source–detector separation. Generally, for smaller breast sizes, lesions of 5-mm diameter could be detected in almost all parts of the compressed breast (parallel-plate geometry) and in the outer parts of the uncompressed breast (cup geometry), whereas for larger breasts, the detection limit moved toward 7.5-mm lesion size when a lesion-to-background absorption contrast of 2:1 was assumed.

The third group of optical breast imagers comprises devices with handheld probes. As an example, Fig. 3(f) shows the probe of the diffuse optical spectroscopic imaging (DOSI) device

developed at the University of California, Irvine.[51,72] This device combines the frequency-domain and the CW approach. It contains two source–detector pairs. The first one is used to perform frequency-domain measurements at six optical wavelengths ranging from 650 to 860 nm. In contrast to the frequency-domain instruments discussed above, the modulation frequency is varied here from 50 to 1000 MHz. Therefore, the amount of information obtained for the sampled tissue volume is comparable to that of time-domain approaches discussed above. The second source–detector pair is connected to a tungsten halogen white-light source and a spectrometer to record broadband reflectance spectra from 650 to 1000 nm. The scatter power law:

$$\mu_s'(\lambda) = \mu_s'(\lambda_0)(\lambda/\lambda_0)^{-b}, \quad (1)$$

which is fitted to frequency-domain data at the six discrete wavelengths, provides a scatter correction for the CW reflectance spectra. In a second step, the absorption spectra are extracted by best fitting the corrected CW reflectance spectra to the photon diffusion model and used to fit the chromophore concentrations. To obtain spatially resolved information, the probe is positioned, e.g., at steps of 10 mm, along a line or a two-dimensional (2-D) grid on the breast at the (known) lesion position with the patient in supine position.[73]

At the University of Pennsylvania, a handheld CW imager was used for breast imaging with a three wavelengths LED source and eight surrounding silicon diode detectors 4-cm apart from the source.[74] Another CW device was developed by ViOptix, Inc., Fremont.[75] Handheld probes have also been used for blood flow characterization in breast tissue and tumors employing diffuse correlation spectroscopy (DCS; cf. Sec. 3.5). A detailed overview about the various handheld NIR devices for breast imaging and other applications can be found in the review by Erickson and Godavarty.[76]

3.2 *Multimodality Imaging*

Several groups have combined optical breast imaging with other clinical breast imaging modalities. Hereby, the conventional clinical modality provides structural information about the breast tissue that is exploited in the reconstruction of the optical and physiological properties. In this way, problems of low spatial resolution and diffuse blurring of reconstructed optical data can be overcome, and optics can provide, e.g., metabolic information about lesions not accessible by the conventional modalities. At the University of Connecticut, a handheld probe device has been developed for combined investigations of breast tumors by NIR light and ultrasound. This probe contains a commercial US detector array together with 12 source and 8 detection fibers for diffuse reflectance frequency-domain measurements at several source–detector distances.[77] In the present version, three optical wavelengths between 660 and 830 nm are used.[78]

The combination of optical and ultrasound measurements in a handheld probe is technically simple, whereas the combination of optical and MR measurements is more challenging. To avoid interference of the optoelectronic components with the high magnetic field, long fibers or fiber bundles have to be used to deliver and collect the light inside the MR bore. Furthermore, the restricted space inside the bore limits the number of source and detector fibers that can be installed. The first demonstration of concurrent optical and MR imaging of breast tissue was reported by Ntziachristos and Ma,[79] who placed a parallel-plate patient interface for time-resolved transmittance measurements inside the MR tomograph. This instrument allowed comparison of contrast-enhanced optical absorption imaging with ICG versus dynamic contrast enhanced MR imaging[80] and provided intrinsic hemoglobin and oxygen saturation contrast StO_2 for malignant and benign breast lesions.[81] At Dartmouth College, a 16 fiber ring holder interface was applied inside the MR scanner for simultaneous frequency-domain optical and MR interventions.[82] During reconstruction of the optical images, the structural information from the MR investigations was used as prior information. This group also reported successfully incorporating water and fat information from MR imaging to improve the accuracy of the reconstructed hemoglobin concentration.[83]

At the Massachusetts General Hospital, a combined optical and x-ray breast imager was developed that uses the parallel-plate geometry. Optical measurements are performed in transmittance by a hybrid frequency-domain and CW approach using a source–detector grid designed for 3-D reconstruction of the optical properties. The device can also be applied for functional monitoring of the breast tissue.[84]

3.3 *Data Analysis and Reconstruction*

One aim of data analysis is the generation of optical mammograms, i.e., the generation of 2-D or 3-D images that display lesions and structures inside the breast with high contrast. Another aim is the determination of the optical and physiological parameters of lesions and of healthy breast tissue. Hereby, the generation of images is not really required. Generally, optical mammograms can provide such values. However, the accuracy of values characterizing lesions is often limited by the diffuse blurring and by partial volume effects. These limitations can be overcome by using prior information about the size and location of the lesions together with adequate heterogeneous models.

The generation of optical mammograms for the circular tomographic geometry requires a reconstruction of the optical or physiological properties of the breast. For the parallel-plate devices, reconstruction can also be applied, but it is not mandatory. Since the distance between source fiber and the detection fiber in scanning devices with parallel-plate geometry is the same at all scan positions, data at each scan position can be analyzed independently.

Figure 4 illustrates some general features of optical mammograms obtained by the various data analysis methods. Transillumination images from parallel-plate instruments [Figs. 4(a)–4(c)] often exhibit not only the carcinoma but also superficial blood vessels and other localized regions of high vascularization. Reconstructed slices from parallel-plate instruments show more blurred structures [Figs. 4(d) and 4(e)]. Similarly, reconstructed images from circular tomographic measurements [Figs. 4(f) and 4(g)] display the carcinoma often within a nonuniform background with additional structures showing high correlation to the source and detector fiber positions.

3.3.1 *Homogeneous models*

Together with time-domain parallel-plate instruments, so-called late-gate and early-gate intensity images are used to generate optical mammograms showing absorbing lesions like carcinomas and lesions with reduced light scattering like cysts with high contrast. Hereby, the different effects of localized scattering and absorbing objects on time-resolved transmittance measurements

are exploited.[90] The late-gate intensity is mostly sensitive to absorption properties, and consequently, a late-gate image at a certain wavelength displays the spatial distribution of the major absorber at that wavelength. Thus, late-gate intensity mammograms at wavelengths around 800 nm are directly correlated to the distribution of (total) hemoglobin in the tissue, whereas late-gate mammograms at wavelength between 650 and 690 nm are more sensitive to the distribution of deoxyhemoglobin in tissue [Fig. 4(a)]. Correspondingly, mammograms taken at about 925 and 975 nm are correlated to the local distribution of lipids and water in the tissue, respectively. In frequency-domain measurements, the absorption properties of tissue are typically displayed by optical mammograms showing demodulation, whereas phase information yields mammograms related to scattering properties. The visual contrast of absorbing objects in late-gate or demodulation images can be enlarged by plotting reciprocal values of these quantities or using a second-derivative method.[53,54,91]

However, simple intensity mammograms at different wavelengths give only qualitative information about optical and physiological properties of lesions. In order to determine these properties quantitatively, time-domain or frequency-domain data have been analyzed by different models of light propagation. A simple approach to determine the tissue optical properties at each scan position is the application of the diffusion model for the homogeneous infinite slab. In this way, optical mammograms showing absorption coefficients and reduced scattering coefficients can be generated. From corresponding data at different wavelengths, maps of hemoglobin concentration HbT and tissue blood oxygen saturation StO_2, water, lipid, and collagen content can be derived relying on Beer's law. Information on number density and equivalent size of the scattering centers (typically cell organelles, membranes, and so on) can be obtained from the dependence of the reduced scattering coefficients on wavelength together with appropriate Mie calculations.[92,93] To improve the robustness and stability of the fitting procedure that aims at estimating a rather high number of unknowns from data collected at few wavelengths, a spectrally constrained global fitting procedure has also been effectively applied.[94] Specifically, the concentrations of oxy- and deoxyhemoglobin, water, lipids, and collagen, together with the reduced scattering coefficient at 600 nm and scattering power b, were fitted directly to time-resolved transmittance curves measured at 7 wavelengths, using the Beer law to relate the absorption properties to the concentrations of the main tissue constituents and the approximation to Mie theory to model the scattering properties.

When a homogeneous model is applied, the contrast between lesions and the surrounding tissue is underestimated since the lesion typically fills only part of the banana-like volume between source and detector (partial volume effect). In order to enhance the contrast in these maps, the application of a second-derivative approach was proposed.[95]

The discussed models for the parallel-plate geometry need to be improved at the edges of the breast since the breast of decreasing thickness no longer fills the space between both glass plates. To avoid artifacts, distributions of times of flight can be scaled using the mean times of flight of the detected photons as a rough measure of the tissue thickness at the various scan positions.[96] This correction works also for fluorescence measurements.[46] In frequency domain, demodulation data can be corrected for edge effects by exploiting the measured phase information.[97]

Measurements in reflection geometry with the handheld probe, as shown in Fig. 3(f), have been analyzed by using the diffusion model for the homogeneous semi-infinite medium.[98]

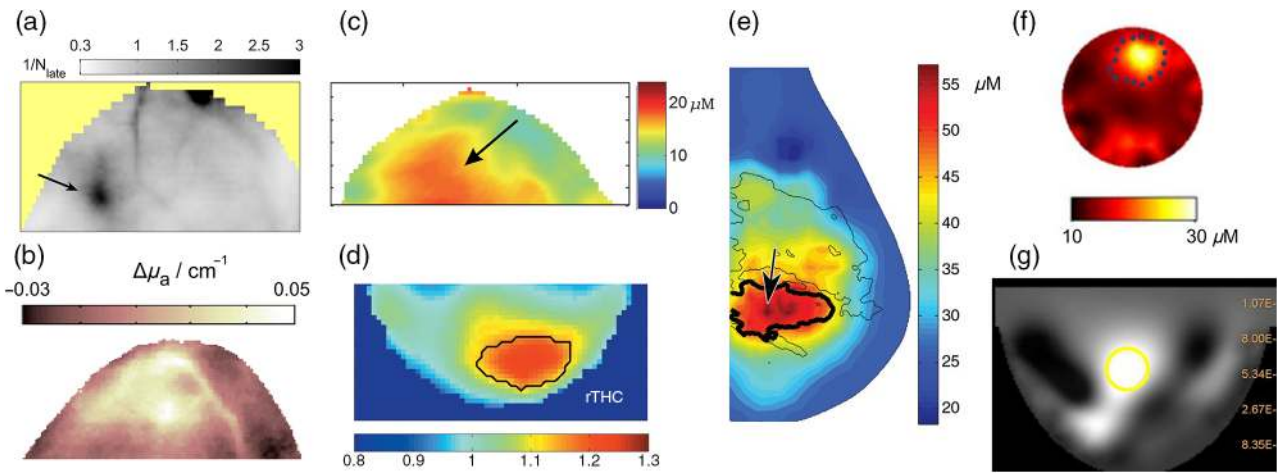

Fig. 4 Examples of absorption and HbT optical mammograms of patients with carcinomas (labeled by arrows or lines): (a) late-gate transillumination image at 670 nm from a parallel-plate instrument displaying a 3.5-cm carcinoma (from Rinneberg et al.[85]); (b) transillumination image at 785 nm from a parallel-plate instrument displaying difference in absorption coefficient $\Delta\mu_a$ from average background analyzed within an inhomogeneous model (from Quarto et al.[86]); (c) HbT transillumination image with 3.9-cm carcinoma from a CW parallel-plate instrument (reprinted with permission from Anderson et al.[87]), (d) reconstructed slice of relative total hemoglobin concentration (designated rTHC) with a 2.2-cm carcinoma from a parallel-plate instrument with matching fluid (reprinted with permission from Choe et al.[47]), (e) reconstructed slice of HbT with a 2.5-cm carcinoma obtained with prior knowledge from x-ray mammography (reprinted with permission of the Radiological Society of North America from Fang et al.[88]), (f) reconstructed slice (HbT map) with a carcinoma about 4 cm in size (reprinted with permission from Wang et al.[65]), and (g) reconstructed absorption image with carcinoma (indicated by yellow circle) from a CW tomographic instrument with matching fluid (image reproduced from van de Ven et al.[89]).

Also, in this analysis, the contrast of the lesion to the surrounding tissue is underestimated due to partial volume effects. By plotting the results obtained at different positions of the probe, a mammogram with a small number of pixels is obtained.[73]

3.3.2 *Heterogeneous models*

More realistic values of lesion optical properties and functional parameters from parallel-plate devices have been obtained by the application of inhomogeneous models considering the lesion as an object in an otherwise homogeneous background medium. One approach is the model of diffraction of photon density waves by a spherical object.[99] Furthermore, a random walk model has been used to derive tumor optical properties.[100] Other approaches are perturbation models like the first-order Born approximation or an empirical Padé approach.[101,102] Since the true shape of the lesion is typically not known, the spherical shape has been assumed in these models. The latter two models have also been employed to generate optical mammograms by assuming a virtual sphere of predefined size located in the midplane of the breast. In this way, the partial volume effect of the homogeneous model discussed above is reduced and the lesion contrast in the optical mammogram is improved. Generally, low order perturbation models are at their limit of validity in a large number of cases, since lesion size and absorption contrast can become large.[103] Recently, a higher order perturbation model has been employed for the analysis of the optical and functional parameters of malignant and benign lesions [see Fig. 4(b)].[86]

The results of the inhomogeneous models strongly depend on the assumptions about the size and the location of the lesion (distance to the parallel plates). The latter information can be easily derived from measurements with offset fibers [cf., Fig. 3(a)].[99] However, the size cannot be reliably determined from the optical measurements due to the diffusive nature of the light propagation. Therefore, often the size information from conventional clinical imaging modalities or from pathological findings has been used as prior information. Hereby, one should have in mind that the extension of the vascular bed of a tumor, which is responsible for the optical contrast, could deviate from the clinical size estimation.

3.3.3 *Reconstruction of optical properties and functional parameters*

Optical mammograms based on the circular tomographic geometry are obtained by 2-D or 3-D reconstruction of optical properties and functional parameters. Typically, the diffusion model is used as forward model. Arbitrary geometries of the breast can be handled by the finite-element method. Time-domain data from the freely pending breast covered by a matching fluid have been analyzed by applying the TOAST software package.[49] At Dartmouth College, a frequency-domain implementation of the finite element method was employed.[104] Later, this model was developed toward a spectrally constrained approach that directly fits the functional parameters, hereby exploiting the scatter power law [Fig. 4(f)].[105] Philips used a back projection algorithm to reconstruct the attenuation coefficients for their CW instrument.[48] In their fluorescence, mammograph reconstruction of attenuation data was performed by a linear Rytov approximation assuming constant scattering [Fig. 4(g)]. For reconstruction of the fluorescence data, a Born approximation was used.[64] Data from the dynamic breast imager of NIRx are analyzed by a linear perturbation method, too.[66]

Data from parallel-plate geometry instruments have also been analyzed by reconstruction. Due to the well-defined breast shape, finite differences on a rectangular grid can be applied here. Ntziachristos et al.[80] used the linear Rytov approximation to reconstruct absorption changes after application of the contrast agent ICG. Since the iteration algorithm did not converge, a calibration procedure was employed.[80] To analyze the CW data from the University of Pennsylvania instrument shown in Fig. 3(b), Culver et al.[106] described an iterative model based on the Rytov approximation of the diffusion equation to reconstruct tissue absorption. Later, data from the University of Pennsylvania instrument were analyzed by a multispectral approach based on finite elements to derive directly the oxy- and deoxyhemoglobin concentrations [Fig. 4(d)].[47] With this multispectral method, the basic problem of separating absorption and scattering properties from CW data could be overcome.[107] The reconstruction method was then extended to analyze fluorescence data recorded with ICG.[60] Dierkes et al.[58] employed a fast linear Rytov approximation to reconstruct both absorption and scattering mammograms from time-domain data. Ziegler et al.[59] developed a nonlinear algorithm based on the Rytov approximation for simultaneous reconstruction of absorption and scattering properties. Another approach for the generation of 3-D optical mammograms in the parallel-plate geometry is the application of tomosynthesis. This method has been applied to both intrinsic contrast and ICG fluorescence contrast investigations.[46]

Reconstruction based on diffusion theory is usually performed with regularization,[108] i.e., the analysis yields a solution of the inverse problem with minimal deviation to a reference dataset, which is either a phantom dataset, e.g., the matching fluid surrounding the breast in several devices, or an average dataset for the breast under investigation. Depending on the grade of regularization, contrast between a lesion and the surrounding tissue could be underestimated. In addition, reduced contrast arising from the blurred appearance of lesions in reconstructed optical images generally limits the accuracy of the optical and functional parameters.

3.3.4 *Reconstruction with prior knowledge*

In multimodality optical breast imaging, the spatial information from the high-resolution modality about tissue structure, in particular, lesion size and location, is used to improve the accuracy of the optical and functional properties of breast lesions derived from the optical data. In this sense, the optical method is used as an adjunct modality that yields functional information about the tissue not accessible by the other modality, whereas the detection of a lesion is based on the nonoptical method. The first step in the analysis is the segmentation of the tissue into the lesion and one or more background tissue types, such as fatty or glandular tissue. Then, reconstruction can be performed either with forcing the optical parameters in these regions to be uniform ("hard prior") or with a "soft prior" approach in which variations of the parameters inside the regions and, in particular, changes across the segmentation boundaries are permitted.

Originally, the hard prior approach was employed. The main advantage of this method is that the number of unknowns in the reconstruction is very small since each tissue type is described by just one parameter vector of optical or functional properties. On the other hand, this approach is very sensitive against errors in the segmentation and deviations in contrast between the imaging modalities. Ntziachristos et al. used the structural

information from MRI to segment the tissue into the suspicious lesion and a surrounding background. The optical properties of the lesion were derived by first order perturbation theory using the Rytov approximation of the diffusion equation.[81]

Brooksby et al.[109] developed a soft prior reconstruction scheme for combined optical and MR imaging with a spatially varying regularization parameter linking the tissue properties of healthy breasts to the reference properties of either adipose or glandular tissue. As in the case of the pure optical measurements at Dartmouth College, a spectrally constrained model based on finite elements was employed for the reconstruction. In recent work, a direct regularization approach was proposed and successfully demonstrated on a patient with breast cancer that no longer requires user-guided image segmentation.[110]

The information from digital mammographic tomosynthesis in the multimodality instrument of the Massachusetts General Hospital was exploited to generate a finite element mesh accounting for the true shape of the breast. Reconstruction of the functional parameters was then performed without prior differentiation of tissue types [Fig. 4(e)]. The structural information was finally applied to assign the reconstructed optical and functional parameters to the different tissue types.[84,88] In early research, the application of different regularization terms for the lesion and background tissue was discussed within the linear Rytov approximation of the diffusion equation.[111] Recently, a compositional approach was tested to analyze data from healthy subjects whereby the tissue at each location was assumed to be a mixture of adipose and glandular tissue.[112] This method has then been extended to subjects with tumors.[113]

The ultrasound data from the combined near-infrared and ultrasound instrument at University of Connecticut are used to segment the tissue into the lesion and background tissue. Then, a grid is defined with a fine voxel size in the lesion and a coarse voxel size outside. Using this grid, the measured frequency-domain data are modeled by a first-order Born approximation for diffuse reflectance in the semi-infinite medium. Hereby, only changes in absorption are taken into account. The total number of voxels corresponds roughly to the number of measurements, and the inverse problem is solved without regularization and without any further differentiation between the lesion and the background voxels.[114] In more recent work, theoretical and experimental attempts have been undertaken to account for the influence of the chest wall that can strongly contribute to the measured signals in the supine position.[115]

3.4 *Broadband Spectroscopy*

Most imagers display mammograms at a limited number of discrete wavelengths, with a minimum of three wavelengths. Operating at seven selected wavelengths (635 to 1060 nm) and applying a perturbative approach for data analysis, it was possible to generate at each wavelength absorption difference $\Delta\mu_a$ maps, with respect to the average absorption of the same breast. From these data, corresponding concentration difference ΔC maps for each tissue constituent (HbR, HbO_2, water, lipid, and collagen) with respect to the average concentration in the same breast were deduced.[86] As an example, in Fig. 5, the adipose nature of the breast is apparent from the high lipid content in the entire breast (in agreement with what was seen in the corresponding x-ray image). As expected based on physiology, the residual of the mammary gland (upper quadrants), which causes marked x-ray attenuation, is characterized by high content of oxygenated blood, water, and also collagen. A blood vessel

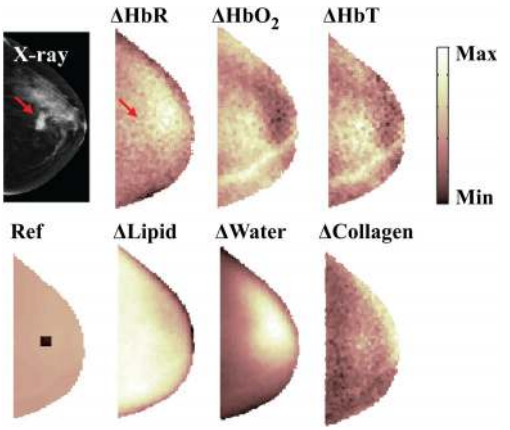

Fig. 5 Concentration difference maps ΔC of the main breast constituents (HbR, HbO_2, HbT, lipid, water and collagen) of the craniocaudal view of the left breast of a patient with a 25-mm invasive ductal carcinoma in the retroareolar area (compressed breast thickness 46 mm); x-ray image (top left) and reference image (bottom left) show carcinoma (red arrow), and lesion area (black square) selected to estimate lesion properties, respectively. The color bar range for ΔC maps depends on the particular constituent, for details, see Quarto et al.[86] (Reprinted with permission of Optical Society of America from Quarto et al.[86])

is clearly detected in the maps of HbT and HbO_2 content, similar to the x-ray image. A carcinoma is characterized by strong hemoglobin, water, and collagen absorption, as confirmed by quantitative estimates in the reference area (see Fig. 5).

In contrast to imagers employing discrete wavelengths, the handheld device developed at the University of California, Irvine, exploits CW broadband operation with halogen lamp illumination covering the range of 650 to 1000 nm together with frequency-domain diode lasers at discrete wavelengths (see Sec. 3.1).[72,98] Tufts University has also recently developed a scanning system that combines CW broadband Xenon arc lamp illumination and detection with a CCD camera coupled to a spectrograph. Spectral images of the compressed breast are acquired every 8 nm between 650 and 950 nm.[87] Although only wavelengths shorter than 850 nm are exploited for data analysis, thus excluding strong absorption peaks of major tissue constituents, the spectral differences among tissue absorbers proved significant enough to allow the estimate of oxy- and deoxyhemoglobin, water, and lipid content.

Some breast studies (e.g., assessment of breast density) aim at quantifying the average properties of breast tissue. Thus, they may not require imaging capabilities. The set-up developed by Lilge and coworkers belongs to the latter category.[116] A halogen lamp was used as a broadband light source, and light transmitted through the compressed breast was collected coaxially and detected by a spectrophotometer coupled to a 2-D CCD camera to achieve continuous operation between 625 and 1060 nm with 3-nm resolution. Measurements were typically performed at four positions on the compressed breast, thus providing some information on breast heterogeneity. Principal component analysis was widely applied to interpret the transmittance spectra, showing that four principal components account for most of tissue variability.[116] Recently, a spectrally constrained global fitting procedure based on photon diffusion has been introduced to estimate the concentrations of HbO_2, HbR, the percentage content of lipid and water.[117]

Another broadband system was also applied to investigate breast tissue composition. It operated in the time domain, scanning continuously between 610 and 1050 nm. A synchronously pumped dye laser and an actively mode-locked Ti:Sapphire laser provided picosecond pulses over the range of 610 to 700 nm and 700 to 1050 nm, respectively, and time-correlated single-photon counting was used to detect the time distribution of either the transmitted or the reflected signal.[118] This was a complex table–top laboratory set-up, not suitable for use in a clinical environment. However, it allowed investigation of breast heterogeneity[119,120] and changes in breast tissue with the menstrual cycle,[121] assessing HbT and StO_2, water and lipid content, and scattering properties. The scattering properties were also further analyzed to estimate the equivalent size of the scattering centers and the anisotropy factor g in the different experimental conditions.

3.5 *Diffuse Correlation Spectroscopy*

DCS is a method to characterize blood flow in tissue, most likely blood flow in the microvasculature.[122] It measures fluctuations in light intensity caused by the movement of scatterers like RBCs. The method employs a near-infrared CW laser with long coherence length to detect the intensity autocorrelation function. The corresponding electric field autocorrelation function is then analyzed to derive a blood flow index. Although a detailed microscopic model relating the drop in the field autocorrelation function with correlation time is missing up to now,[123] changes in this index are taken as a quantitative measure for changes in blood flow.[122] The drop in the field autocorrelation is best fitted to a Brownian motion model, rather than a random flow model. Choe et al.[124] used a two-fiber handheld probe with a source–detector separation of 2.5 cm to perform DCS measurements on breast tissue in reflection. This probe was moved along a line crossing the lesion of interest. In a study by Busch et al.,[125] DCS was applied for measuring the blood flow index in transmission through the breast, which was strongly compressed similar to the conditions in x-ray mammography.

4 Clinical Results

4.1 *Detection and Characterization of Breast Cancer*

One of the fundamental questions of optical breast imaging is how this technique can contribute to diagnosis and therapy control of breast cancer, either as a stand-alone method or as an adjunct modality to conventional imaging modalities. The potential of the technique depends, in particular, on differences in the optical and functional properties of healthy breast tissue and of the various types of malignant and benign lesions. Since optical and functional properties of breast tissue show large intersubject variability, relative changes are of particular interest.

First, exploratory studies with the various imaging devices discussed in Sec. 3 had been conducted as case studies with a small number of patients. Hereby, breast carcinomas were found to show a large increase in HbT, whereas benign lesion exhibited a smaller enhancement.[81,126–129] When tissue blood oxygen saturation StO_2 was determined, a reduced value was reported for carcinomas compared to normal breast tissue as result of the initial studies.[81,126–128] The first observation corresponds to the increased vascularization of carcinomas due to neoangiogenesis and circumferential growth. The reduced oxygen saturation was interpreted as an indication of a high metabolic rate in carcinomas. However, as will be discussed below in some detail, larger studies revealed that a considerable number of breast tumors are characterized by an increase in tissue blood oxygen saturation, i.e., vascular oxygen supply may overcompensate transvascular oxygen loss and tissue metabolic oxygen consumption.

Over the years, clinical results on a large number of subjects have become available.[47,72,86–88,130–133] Table 1 summarizes cohort average values of functional properties for lesions and healthy tissue that have been published by several research groups. Table 2 lists results on tumor-to-normal tissue contrast (given as relative values or differences), which represent averages of individual contrast values taken over the patient cohort investigated. It has to be taken into account that instrumental characteristics, methods of data analysis, and clinical protocols differed significantly among studies. Thus, results obtained from different studies are often difficult to compare quantitatively. Despite this caveat, more recent and extended studies confirmed the expectation concluded from tumor neoangiogenesis that breast carcinomas have an increased content of hemoglobin compared to host tissue. Average values of this increase range from about 15%[47] to 200%.[134,135] In tendency, smaller values are typically obtained by the application of a homogeneous model[72,131] or by reconstruction,[47,88,136] whereas heterogeneous models yield larger ratios.[86,134,135] The ratio $HbT_{(T)}/HbT_{(N)}$ reflects large intersubject variability. Figure 6(a) gives an example of the data spread from a study on 87 carcinomas analyzed by a heterogeneous model.[134] High intersubject variability was also confirmed by Fang et al.,[88] who detected statistically significant difference in HbT when malignant lesions are compared with healthy tissue in a paired test but not in an unpaired test.

Average data for benign lesions, such as fibroadenomas and fibrocystic changes, show a smaller increase in HbT than carcinomas[86,133] or no significant differences at all.[47] However, particular benign mastopathic alterations in the breast can result in a large contrast in HbT images.[138] In a study on about 150 patients with suspicious lesions, only 40% of the histologically confirmed carcinomas dominated the contrast in the optical mammogram.[85] In the other cases, either benign lesions or highly vascularized tissue regions showed up with higher contrast. Accordingly, the specificity of optical breast imaging as a stand-alone imaging modality was found to be poor.[52,69,85]

The initial result that carcinomas generally exhibit lower tissue blood oxygen saturation was not confirmed later by several larger studies. The clinical studies performed during the European OPTIMAMM project on optical mammography have shown that, on average, tissue blood oxygen saturation StO_2 in breast carcinomas is not noticeably reduced.[134,135] This observation has then been confirmed by studies of other groups.[47,72,88] As illustrated by the data in Fig. 6(b), there are carcinomas with StO_2 above ($StO_{2(T)} > StO_{2(N)}$) and below ($StO_{2(T)} < StO_{2(N)}$) normal. As discussed above, tissue blood oxygen saturation reflects the balance between oxygen influx, i.e., oxygen supply, and oxygen transvascular flux or tissue metabolic rate of oxygen consumption, i.e., oxygen demand. This balance depends on the tumor vascular network obtained by remodeling of the host vascular network following vessel cooption, angiogenesis, circumferential growth, and regression of tumor vessels. Breast tumors with tissue blood oxygenation above normal

Table 1 Functional properties of malignant and benign breast lesions (N = number of patients, FAD = fibroadenoma) and of healthy breast tissue from *in vivo* tissue optical spectroscopy.

		Healthy	Malignant		Benign	
Property	References	Mean ± SD	Mean ± SD	N	Mean ± SD	N
HbT (μM)	Grosenick et al.[134]	17.3 ± 6.2	53 ± 32	87		
	Spinelli et al.[a]	12.6 ± 5.9	68.8 ± 94.3	32		
	Cerussiet al.[72]	17.5 ± 7.5	24.7 ± 9.8	58		
	Zhu et al.[130]	—	71.9 ± 18.8	61	39.1 ± 14.9	114
	Fang et al.[88]	19.2 ± 6.5	27.2 ± 13.9	26	24.3 ± 12.3	17 (solid)
					23.0 ± 12.6	8 (cyst)
StO_2 (%)	Grosenick et al.[134]	74 ± 7	72 ± 14	87		
	Spinelli et al.[a]	71.3 ± 17.6	76.5 ± 10.0	32		
	Cerussi et al.[72]	67.7 ± 9.3	67.5 ± 8.4	58		
	Fang et al.[88]	73 ± 6	74.8 ± 6.5	26	76.4 ± 5.2	17
Water (%)	Cerussi et al.[72]	18.7 ± 10.3	25.9 ± 13.5	58		
Lipids (%)	Cerussi et al.[72]	66.1 ± 10.3	58.5 ± 14.8	58		
Scatter power b	Grosenick et al.[134]	0.99 ± 0.35	1.38 ± 0.71	29		
	Spinelli et al.[a]	0.88 ± 0.39	0.79 ± 0.56	32		
		0.82 ± 0.60			0.98 ± 0.76	14 (FAD)
		0.93 ± 0.60			1.56 ± 0.90	40 (cyst)
	Cerussi et al.[72]	0.58 ± 0.23	0.72 ± 0.32	58		
	Fang et al.[88]	0.91 ± 0.01				

[a]Reference 135 and P. Taroni (private communication).

[$StO_{2(T)} > StO_{2(N)}$, see Fig. 6(b)] may be associated with high tumor blood flow through large-diameter tumor blood vessels, whereas breast tumors with StO_2 below normal ($StO_{2(T)} < StO_{2(N)}$) may indicate restricted perfusion at least in parts of the tumor vasculature or high oxygen consumption in tumor tissue. A plot of tumor blood oxygenation $StO_{2(T)}$ versus total hemoglobin concentration $HbT_{(T)}$ on a patient by patient basis [see Fig. 5(a) of Ref. 134], corresponding to the data illustrated in Fig. 6, shows lower tumor blood oxygenation at smaller total hemoglobin concentrations and $StO_{2(T)}$ to approach an upper limit at high total hemoglobin concentrations ($HbT_{(T)}$). This observation indicates that perfusion (rBF) and total hemoglobin concentration (HbT), or vascular volume density (rBV), are positively correlated. Similarly, a scatter plot of tumor to normal oxygen saturation $rStO_2 = StO_{2(T)}/StO_{(N)}$ versus tumor to normal total hemoglobin concentration $rHbT = HbT_{(T)}/HbT_{(N)}$ on a case by case basis reveals that tumors with tissue blood oxygen saturation falling below normal are associated with only small increases in total hemoglobin concentration, whereas tumors with StO_2 above normal exhibit larger increases in HbT.[134,139] This spread in $rStO_2$ shows tumor-to-normal blood oxygen saturation obtained from diffuse optical imaging to be unsuited for tumor versus normal discrimination. Furthermore, conventional diffuse optical imaging probes intravascular oxygen concentration, it does not directly assess tissue partial oxygen pressure and hence cannot detect tumor hypoxia. Saturation data for benign breast lesions were found to be in the range of the values for healthy breast tissue.[47,86,88] Recently, a study on 26 breast cancer patients employing CW spectroscopic imaging (650 to 850 nm) yielded lower tissue blood oxygenation by $\Delta StO_2/StO_{2(N)} = -5\%$.[87] However, scattering was not measured for each patient separately but was accounted for by using literature values both for the reduced scattering coefficient at a reference wavelength and for the scattering power to estimate the scattering spectrum, raising doubts on the accuracy of the results obtained.

Statistically relevant data on water and lipid concentrations in carcinomas were first published by Cerussi et al., who employed a combined frequency domain and broadband spectroscopy system, using, however, a smaller source–detector distance than other groups. In this way, sufficient signal-to-noise-ratio could be reached at wavelengths above 900 nm. Water concentration was found to be larger in carcinomas, whereas lipid concentration was smaller in carcinomas than in normal tissue of the same breast.[72] Recently, Quarto et al. reported similar results obtained from a parallel-plate breast scanner. Additionally, they reported

Table 2 Differences or ratios of functional properties between malignant or benign breast lesions (N = number of patients) and healthy breast tissue. Data represent average values of the individual contrast data. Values in parentheses were calculated from the cited papers by the authors of this review.

			Malignant		Benign	
Property	References	Parameter	Mean ± SD	N	Mean ± SD	N
Hemoglobin	Grosenick et al.[134]	rHbT	2.5 ± 1.6	87		
	Cerussi et al.[72]	ΔHbR	4.62 μM	58		
		ΔHbO_2	7.90 μM			
	Zhu et al.[130]	rHbT (malignant versus benign)	(≈2)	61		114
	Choe et al.[47]	rHbT	1.16	37	0.98	10
		rHbR	1.18		1.11	
		$rHbO_2$	1.14		0.94	
	Fang et al.[88]	rHbT	1.37 ± 0.29	26	1.19 ± 0.27	17 (solid)
					1.06 ± 0.17	8 (cyst)
	Quarto et al.[137]	ΔHbR	5.15 μM	45	3.57 μM	38
		ΔHbO_2	5.76 μM		4.56 μM	
	Anderson et al.[87]	ΔHbT	2.4 ± 0.4 μM			
		ΔHbR	1.2 ± 0.2 μM			
		ΔHbO_2	1.1 ± 0.3 μM			
StO_2	Grosenick et al.[134]	$rStO_2$	(≈0.97)			
	Cerussi et al.[72]	$rStO_2$	(≈1.0)	58		
	Choe et al.[47]	$rStO_2$	0.98	37	0.96	10
	Fang et al.[88]	$rStO_2$	1.01 ± 0.03	26	1.01 ± 0.07	17
	Anderson et al.[87]	ΔStO_2	−5 ± 1%			
Water	Cerussi et al.[72]	Δ%	13.3%	58		
	Quarto et al.[137]	Δ%	11.12%	45	9.95%	38
	Anderson et al.[87]	Δ%	7 ± 1%			
Lipids	Cerussi et al.[72]	Δ%	−14.1%	58		
	Quarto et al.[137]	Δ%	−15.57%	45	−10.95%	38
	Anderson et al.[87]	Δ%	−8 ± 2%			
Collagen	Quarto et al.[137]	Δ%	58.25%	45	31.75%	38
μ_s'	Grosenick et al.[134]	$r\mu_s'$ (785 nm)	1.2 ± 0.4	87		
	Choe et al.[47]	$r\mu_s'$ (786 nm)	1.53	37	0.98	10
	Fang et al.[88]	$r\mu_s'$ (830 nm)	1.18 ± 0.34	26	1.07 ± 0.14	17 (solid)
					1.03 ± 0.04	8 (cyst)

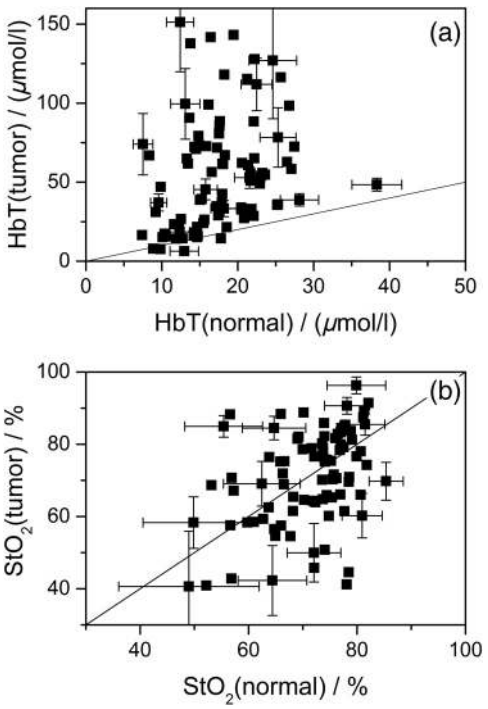

Fig. 6 (a) Total hemoglobin concentration and (b) oxygen saturation of 87 carcinomas plotted versus the corresponding reference value of healthy tissue of the same breast (from Grosenick et al.[134]).

corresponding data for benign lesions, showing the same qualitative trend but less marked differences than in the case of malignant lesions with respect to normal tissue.[86]

In order to account for the increased Hb and water concentration and for the decreased lipid concentration in a single parameter, the following tissue optical index was proposed to achieve high contrast for carcinomas:[72]

$$\mathrm{TOI}_1 = \frac{\mathrm{HbR} \times \mathrm{Water}}{\mathrm{Lipid}}, \tag{2}$$

where HbR denotes tissue deoxyhemoglobin concentration. To account for intersubject variability, Choe et al.[47] adopted the relative tumor-to-normal ratio rX of each measured parameter, instead of its absolute value X. To discriminate malignant from benign lesions, they proposed the optical index:

$$\mathrm{TOI}_2 = \frac{r\mathrm{HbT} \times r\mu_s'}{r\mathrm{StO}_2}, \tag{3}$$

which relies on relative values and combines variables in agreement with the expected tumor neoangiogenesis and higher tissue cell density. However, according to the discussion given above, relative tissue blood oxygenation $r\mathrm{StO}_2$ appearing in the denominator may not improve discrimination.

In recent years, it is becoming more common to try not only to detect optical contrast between breast lesions and healthy tissue but also to correlate optically assessed macroscopic parameters with microscopic information on tumors (e.g., grade, proliferation), even though up to now this has often been attempted only on small patient cohorts. Broadband CW acquisition was performed by Anderson et al.[87] on 26 breast cancer patients. They observed significant correlation between the optical contrast due to the different tumor-to-normal tissue composition and the tumor grade as quantified by Nottingham histologic score, which is a measure of tumor aggressiveness and is used to guide therapy and predict its outcome. Water content showed the strongest correlation and HbT the weakest one. Interestingly, no significant correlation was observed between optically derived parameters and tumor size, which is expected to increase optical contrast, as a homogeneous model was used for data analysis.[87] At the University of Pennsylvania, Chung et al.[140] investigated the correlation of optically estimated blood parameters with the expression of Ki67 (proliferation marker, $N = 18$) and CD34 (angiogenesis marker, $N = 19$). Positive correlation was observed between StO_2 and Ki67 expression (which is used to predict patient prognosis and response to chemotherapy), and between HbT and mean vessel area. At Dartmouth College, exploring optical tomography for monitoring of NAC (see Sec. 4.4) in 11 subjects, significant correlation was observed between pretreatment HbT values and expression of CD105 (marker of tumor-induced blood vessels) only in subjects that turned out to be responders to therapy.[141] These outcomes suggest that complex information can be obtained noninvasively by optical means, and further work is needed to understand it in depth and to fully exploit its potential.

Several clinical studies have shown that, on average, the reduced scattering coefficient of carcinomas is larger than that of healthy tissue. Fang et al.[88] and Grosenick et al.[134] observed an increase by about 20%, Choe et al.[47] even by about 50%. Higher scattering in malignant lesions than in benign lesions, or healthy tissue, also agrees, at least qualitatively, with the results of a small pilot study performed to compare optically assessed scattering properties with the pathologic analysis of microscopy images of cellular morphology.[142] As shown in Table 1, several groups have measured, in particular, higher scatter power coefficients b in carcinomas than in healthy tissue. Different results on the scattering properties of carcinomas have been reported by Spinelli et al.,[135] who observed a reduction of scatter power and also a slight reduction of μ_s', possibly indicating that the limits of perturbation theory used for data analysis had been reached. For solid benign lesions, either no significant change[47,135] or a small increase of μ_s' was reported.[88]

Recently, the concentration of collagen was considered as a further parameter for the characterization of carcinomas and benign lesions. Based on data from 62 patients with carcinomas or benign lesions, Quarto et al.[86] described a large increase of the collagen concentration in carcinomas compared to a smaller increase in benign lesions and supposed that collagen might have high diagnostic relevance. Taking tissue absorption by collagen into account reduces the total hemoglobin concentration and increases StO_2 since collagen contributes to tissue absorption not only above 900 nm but also below 700 nm.[143]

Choe et al.[124] employed DCS to investigate the microvascular blood flow of healthy tissue and malignant breast lesions. Results on 32 subjects revealed on average a 2.25-fold larger blood flow index for malignant lesions compared to normal tissue of the same breast. Similar results were obtained when the contralateral breast was used as reference, which implies that malignant tumors have significantly higher blood flow than normal tissue.

Several papers discussed optical properties of (liquid filled) cysts. These lesions could be distinguished from carcinomas and solid benign lesions by their smaller reduced scattering coefficient.[85,135,144] By contrast, Fang et al.[88] did not see such a

reduction. Instead, these authors reported a significantly reduced StO_2 value in cysts as compared to healthy tissue and to other lesions.

Statistical tests performed on the discussed composition and functional properties of carcinomas, healthy tissue and benign lesions revealed significant differences leading to the conclusion that these properties are suited to diagnose carcinomas and to differentiate between malignant and benign lesions, different from what was suggested by earlier studies.[52,69,85] Accordingly, high sensitivity and specificity values for optical imaging were obtained: e.g., when HbT is used as criterion for diagnosis, Choe et al.[47] reported a sensitivity of 98% and a specificity of 90% and Zhu et al.[130] obtained a sensitivity of 92% and a specificity of 93%. Chance et al.[74] detected 44 carcinomas from 116 subjects with a sensitivity of 96% and a specificity of 93% by using HbT and StO_2. However, the latter results should be taken with caution since only CW radiation at three different wavelengths was used and separation of absorption from scattering thus was difficult. Also, Deng et al.[113], exploiting data fusion on x-ray imaging and optical tomography to build HbT maps, were able to differentiate 30 malignant from 24 solid benign lesions ($p = 0.006$ in a two-sample t-test). For the discrimination between 16 malignant and 9 benign lesions, Zhao et al.[145] tested both HbT and the tissue optical index:

$$\mathrm{TOI}_3 = \frac{\mathrm{HbT} \times \mathrm{Water}}{\mathrm{Lipid}}, \tag{4}$$

which were obtained from MRI-guided diffuse optical tomography. They achieved an area under the curve (AUC) of 0.79 and 0.94, respectively, suggesting that by additionally taking into account, tissue composition besides total hemoglobin can improve the diagnostic potential. Mastanduno et al.[146] analyzed 30 patients from the same study and reported an increase in specificity from 67% for MRI to 89% when results from MRI and TOI_3 are combined. Along this line, Kukreti et al.[147] exploited the system developed at the University of California, Irvine, to investigate spectral differences between malignant, benign, and healthy breast tissue over a broad spectral range. This allowed them to identify minute (ppm) spectral signatures observed in malignant tissue that cannot be accounted for by hemoglobin, water, and lipids. Exploiting this "specific tumor component," they were able to discriminate between malignant ($N = 22$) and benign (fibroadenomas, $N = 18$) lesions with sensitivity of 91% and specificity of 94%. However, to our knowledge, this approach has not been followed any further.

When interpreting the high values of sensitivity and specificity reported, one should have in mind that they were in part derived by exploiting prior knowledge about the existence and even the location of the lesion. The task of optical imaging focuses on determining functional parameters for tissue regions defined by other modalities. This approach differs from the original attempts of optical mammography that aimed at the detection of lesions from the optical image itself and that revealed a low specificity of the optical method.[52,55,131,148] With lesion position known from a conventional breast imaging modality, tissue regions with high contrast in optical mammograms that do not coincide with the position of the known lesion in the conventional modality are ignored. This approach avoids, in particular, the problem of low specificity and yields values above 90%.

Generally, the high values for sensitivity and specificity are encouraging to use optical imaging as an adjunct modality to conventional breast imaging. The various clinical studies have shown that HbT, water, lipid and collagen concentration, the scattering properties, and related parameter combinations can potentially be exploited to improve the workflow in breast cancer diagnosis.

4.2 *Dynamic Response to External Impact*

The work on the detection and differentiation of breast tumors discussed so far was related to properties of breast tissue under static conditions. There have been several attempts to induce dynamic changes of the intrinsic functional properties in order to discriminate malignant from benign lesions and from healthy breast tissue. With respect to the origin of the optical contrast, one can distinguish between (1) alterations that primarily vary blood volume and blood flow and (2) alterations that primarily affect blood oxygen saturation. Due to their disorganized vasculature and the particular metabolism of cancer cells, carcinomas should show a different transient response with respect to healthy tissue and possibly to benign alterations.

Schmitz et al.[66] proposed a Valsalva maneuver, which was expected to temporarily increase the Hb concentration in the breast due to vein congestion. Using their dynamic dual-breast imager, a single case study revealed a significantly slower recovery of the reconstructed HbR concentration after the end of the breath hold for a carcinoma compared to the contralateral healthy breast. More recently, measurements on two patients with carcinomas using a novel instrument confirmed the sluggish recovery that reflects the increased resistance of the tumor vasculature to blood flow.[149]

Blood volume and blood flow can also be varied by the application of external pressure to the breast. The parallel-plate instrument ComfortScan of DOBI Medical International Inc. temporarily applies a pressure of 10 mm Hg to the breast tissue in order to affect cessation of blood flow in the abnormal capillaries of malignant tumors. The local trapping of RBCs is expected to cause a fast reduction of StO_2 compared to healthy tissue and benign lesions, where blood flow is still going on. Such a reduction is observable by a reduction of light transmission around 640 nm. A multicenter clinical trial revealed 74% sensitivity and 92% specificity.[150] In a recent study, a sensitivity and specificity of 80% and 87% were obtained, respectively.[151] Furthermore, a study on 617 young women showed a sensitivity of 98% and a specificity of 87%.[152] The applied pressure of only 10 mmHg should be compared to the elevated interstitial pressure in breast carcinomas known to rise up to 30 mmHg or even higher.[13]

Xu et al. used a handheld probe with CW light sources and an integrated load sensor to temporarily increase the pressure on top of a lesion known from ultrasound for 10 s. However, measurements on 36 cases did not reveal any significant decrease in StO_2 originating from the pressure change.[153]

A temporal change in blood oxygen saturation can be induced by changing either the oxygen or the carbon dioxide (CO_2) concentration in the inhaled gas. Enhanced oxygen inhalation results in a global increase of StO_2, which then causes vasoconstriction. Enhanced CO_2 leads to a right shift of the oxy-Hb dissociation curve corresponding to a decrease in StO_2, which finally results in vasodilation. Carpenter et al. used these effects in a pilot study on two patients with carcinomas. The patients received inhalation gas during four cycles, each cycle corresponding to 2 min 100% O_2 supply followed by 2 min of carbogen gas (95% O_2, 5% CO_2). Using MR-guided

optical imaging, normal tissue showed a stronger modulation between decreased HbT due to vasoconstriction and enhanced HbT due to vasodilation than the carcinomas. This difference was probably an indicator for the lack of adequate response of smooth muscle cells in the carcinoma vessels required for adapting the vessel diameters. Furthermore, strong temporal delays between the vessel diameter modulation in the healthy and the tumor tissue were observed.[154] Using a CW transillumination method, Dixit et al.[155] investigated patients with malignant and benign breast lesions, who were inhaling carbogen. However, the results on temporal changes in HbO_2 and HbR for the various lesions derived by an eigenvector approach did not clearly show common features of the lesions. A general increase in oxygenation visible in healthy as well as diseased subjects was explained by the increased oxygen content in carbogen compared to air. The difficulties of Dixit et al. to observe a robust hemodynamic response by using carbogen are in line with a study on healthy subjects by Carpenter et al.,[156] who reported that air/carbogen as well as air/oxygen breathing yield less robust data than the oxygen/carbogen modulation method.

The effects of pressure-induced changes in breast tissue were also investigated in a number of studies, on healthy subjects, mainly, to understand changes in the tissue functional parameters by compression plates or pressure-induced optode coupling to tissue. In a first study on five healthy subjects, Jiang et al.[157] reported that the pressure of a circular optode arrangement on the tissue results in an increase of HbT and StO_2 and in a decrease of the tissue water content. By contrast, a later study of this group on 17 healthy subjects revealed a decrease of HbT and no significant alterations in StO_2 and water concentration.[158] Similar to the latter result, Carp et al. observed a decrease in HbT when using high compression in their parallel-plate combined optical and x-ray approach. Moreover, a decrease in StO_2 and μ_s' was observed.[159,160] The reduced HbT indicates that due to higher pressure blood is partly pressed out of the breast vasculature. Furthermore, for high compression similar to x-ray mammography, a strong reduction in blood flow of about 88% was observed using DCS measurements.[125] Altogether, these results indicate that tissue compression could reduce optical imaging contrast hampering the detection of tumors. Busch et al.[125] report on a noticeable effect of soft tissue compression. On the other hand, results on tumor contrast obtained with soft tissue compression did not noticeably differ from data obtained with pressure-free techniques. This is also the case for dynamic measurements using a bolus of ICG (cf. next section).

4.3 *Exogeneous Contrast Agents and Fluorescence Mammography*

The results on endogeneous tissue contrast discussed in Secs. 4.1 and 4.2 show several promising features that could be helpful in breast cancer diagnosis. However, they did not yet reveal sufficient potential to substantially change the clinical workflow in diagnostic mammography. Exogeneous contrast agents offer the possibility to exploit contrast mechanisms that are superior to endogeneous tissue contrast and, therefore, could help to improve cancer detection and differentiation. In particular, molecular imaging has been discussed and investigated for the past decade as a new way for early detection of tumors with high specificity.

However, the development and approval of a new dye suited for applications on human subjects is a long and expensive process. So far, two contrast agents have been applied in optical imaging studies on patients with breast cancer. The first one is the well-known NIR dye ICG, which is routinely used in clinical practice for other applications (e.g., hepatic function and ocular fundus fluorescence angiography) since many years. ICG has been approved by regulatory agencies for investigation of the microcirculation yet has not been approved for fluorescence imaging of the breast. The second dye is a newly developed substance with the name omocianine, which does not have any approval for medical applications so far.

ICG can be detected in the breast by its absorption around 760 nm as well as by its fluorescence around 830 nm. The pharmacokinetic behavior is well known. After intravenous injection, ICG quickly binds to high molecular weight plasma molecules like lipoproteins. Within typically less than 10 min, the dye is cleared from the blood by the liver.

A first application of this dye in optical mammography was reported by Ntziachristos et al.,[80] who reconstructed the change in absorption observable about 3 min after intravenous injection of a bolus of ICG. Optical imaging was restricted to a tissue slice selected from concurrent Gd-enhanced MRI taken in the same parallel-plate geometry as the optical imaging. Investigations on two subjects with a malignant (1-cm invasive ductal carcinoma) and a benign (1.5 cm fibroadenoma) lesion showed good spatial correlation of high ICG absorption with the Gd enhancement visible for both lesions. Outside the lesions, areas with smaller ICG enhancement were visible, similar to moderate enhancement obtained for the healthy case. The possible benefit of the ICG enhanced absorption with respect to the measured intrinsic lesion absorption was not considered by the authors.

Intes et al.[161] measured the full-time course of ICG uptake and washout on three patients using a single-wavelength CW imager. The circular arrangement of sources and detectors on the freely pending breast was positioned according to the expected lesion position determined from palpation. Figure 7(a) displays the time courses obtained from reconstruction of absorption changes using a perturbation approach. The two malignant cases show a significantly slower inflow and wash-out in comparison to the benign lesion and to the surrounding normal tissue. This slower inflow and wash-out likely indicated the increased resistance to blood flow arising from the chaotic vessel structure in the carcinomas, and possibly indicated extravasation of ICG.[161]

Rinneberg et al.[85] used the first generation PTB parallel-plate optical mammograph to investigate the time course of ICG absorption after bolus injection for 11 patients with suspicious lesions. These measurements showed distinct patient-to-patient variations of the wash-out curves. However, the temporal characteristic for the carcinoma and healthy tissue of the same breast was almost identical in all cases. As an example, Fig. 7(b) shows the time courses for a 2-cm invasive ductal carcinoma and for two reference positions within the surrounding normal tissue, chosen on different sides of the tumor. In each case, ICG absorption has been normalized to the HbT value measured at the same location of the breast. Since the three curves fall on top of each other after normalization, ICG absorption is proportional to absorption by hemoglobin. This observation reflects the known strong binding of ICG to blood plasma proteins, which hinders extravasation of the dye molecules. The authors concluded that the investigation with ICG yields essentially the same tumor absorption contrast as accessible from the intrinsic total hemoglobin concentration.

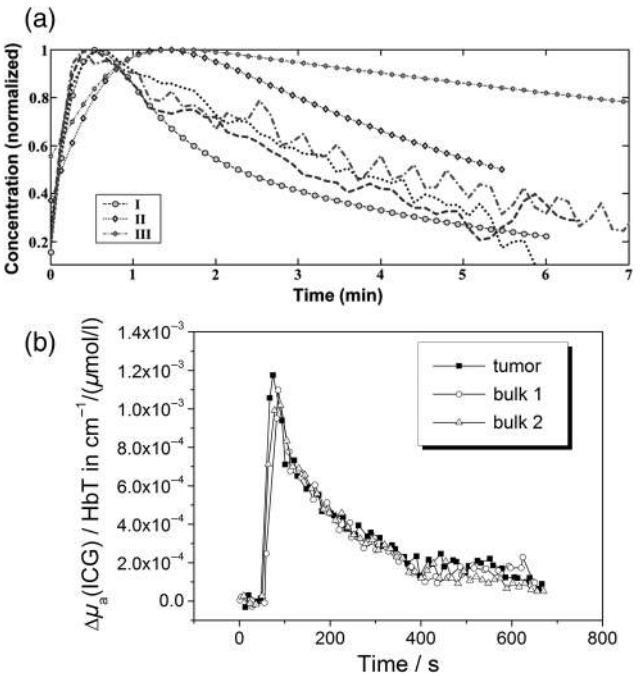

Fig. 7 (a) ICG inflow and washout characteristics after bolus injection for three patients with breast tumors measured by Intes et al.;[161] case I: fibroadenoma (diameter 1 to 2 cm), case II: adenocarcinoma (diameter 2 to 3 cm), case III: invasive ductal carcinoma (size 4 cm × 3 cm) (reprinted with permission of American Association of Physicists in Medicine from Intes et al.[161]); (b) time courses of ICG absorption after bolus injection normalized to HbT for a 2-cm invasive ductal carcinoma and two healthy reference locations measured by Rinneberg et al.[85]

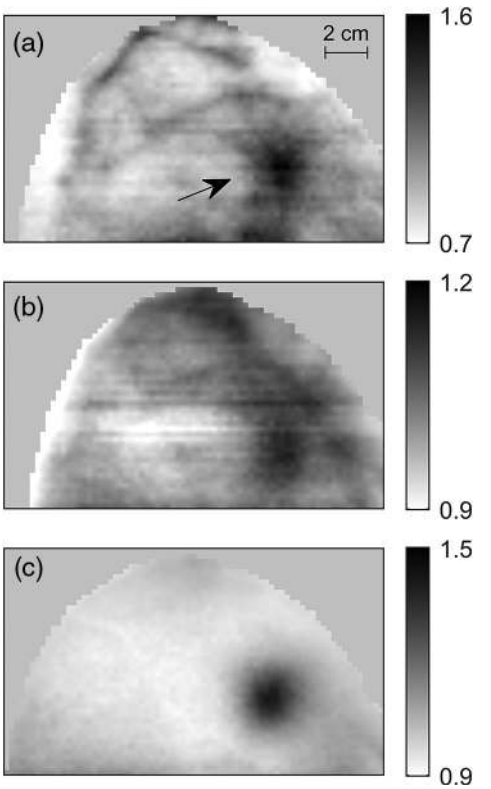

Fig. 8 Optical mammograms of a patient with an invasive ductal carcinoma (arrow) from the study of Hagen et al.:[162] (a) absorption (normalized late-gate intensity) at 660 nm without contrast agent, (b) ICG fluorescence during dye infusion, and (c) ICG fluorescence after washout of the dye from the vessels.

In 2007, Corlu et al.[60] demonstrated that ICG can be detected in breast cancer by fluorescence measurements. The investigations were performed with the frequency-domain/CW parallel-plate instrument of the University of Pennsylvania equipped with spectral filters for fluorescence detection by the installed CCD camera. Fluorescence data were acquired in a time window from 6 to about 16 min after injection of the ICG bolus. Images of the ICG concentration at 10.2 min after ICG injection and of other functional parameters, such as HbT, StO_2, and μ_s' were derived by 3-D reconstruction. Data on three patients with invasive ductal carcinomas revealed a lesion-to-background contrast in the reconstructed ICG concentration of 4:1 to 6:1 compared to about 1.3:1 contrast in HbT and typically, 1.5:1 contrast in μ_s'. The strong difference in the ICG and HbT concentration contrast was discussed as an indicator for extravasation of ICG due to leaky tumor vasculature.[60] This result disagrees with the data of Rinneberg et al. displayed in Fig. 7(b), which exhibits similar contrast for ICG and HbT about 10 min after bolus injection. As discussed above, extravasation was negligible within the considered 10-min time window after bolus injection for the 11 cases investigated in this study.[85]

In 2009, first results of a clinical study with the PTB fluorescence mammograph were published in which extravasation of ICG in carcinomas was explicitly exploited as contrast mechanism.[162] This study differed in two main aspects from all previous investigations discussed above. First, the ICG concentration was not only measured during the washout period but also, at a later time at which no more ICG could be seen circulating through the blood vessels. Second, the ICG bolus was followed by a typically 20 min lasting period of constant ICG infusion. The aim of this infusion was twofold. It should allow for a measurement at constant ICG concentration in the vascular compartment during infusion to avoid difficulties arising from the continuous drop of the ICG concentration following a bolus injection during image acquisitions times of several minutes. Furthermore, ICG infusion over an extended period of time should increase ICG extravasation compared to the application of a bolus followed by rapid ICG clearance from blood by the liver. Figure 8 illustrates the results obtained at different times of the investigation for a patient with an invasive carcinoma. The mammogram in Fig. 8(a) shows the late-gate intensity absorption contrast at 660 nm before injection of the dye, Fig. 8(b) shows the ICG fluorescence signal that was measured during the infusion period, and Fig. 8(c) shows the ICG fluorescence signal recorded about 25 min after the infusion had been stopped.

The first two images exhibit essentially the same structures in the breast. In Fig. 8(a), the carcinoma as well as several blood vessels are visible due to the corresponding hemoglobin absorption (at 660 nm mainly deoxy-Hb), and in Fig. 8(b), the same structures are visible from fluorescence since the ICG is contained almost entirely in the vasculature inside and outside the carcinoma. The situation changes dramatically in Fig. 8(c). Now, the ICG from the vessels has been washed out completely, and the small amount of ICG that extravasated through the leaky vessel walls of the carcinoma becomes visible. A study on 20 patients showed that ICG extravasation occurs only for malignant and not for benign tumors.[163] This result is in accordance with the EPR effect of macromolecules in solid

carcinomas. ICG, which strongly binds to the lipoproteins in the blood, acts as a fluorescent label for these macromolecules. Such macromolecules can extravasate in carcinomas due to the leakiness of the vessels and remain there for an extended period of time. Interstitial flow is reduced due to the impaired lymphatic system. By contrast, the vasculature in the benign lesion was not permeable for the ICG-labeled macromolecules. Hence, fluorescence mammography with ICG offers a way to differentiate malignant from benign lesions in the breast, which is a clear advantage compared to measurements exploiting the intrinsic tissue contrast only.

The dye omocianine mentioned above, also known under the name tetrasulfonated carbocyanine dye, does not show strong binding to blood plasma proteins.[164] This contrast agent circulates more than 24 h through blood vessels.[64] So far, it was used in two dose finding studies. Investigations on 52 patients were performed in a multicenter study with a prototype CW fluorescence mammograph from Imaging Diagnostic Systems, Inc. (Ft. Lauderdale, United States).[165] This study revealed considerable variations in sensitivity at different omocianine concentrations. At the dose optimum, a detection rate of 100% was found for malignant lesions, whereby a large number of additionally visible lesions indicated low specificity. Van de Ven et al.[64] reported on a study with omocianine performed with the Philips fluorescence mammograph. Dye enhancement was observed in lesions as well as in glandular tissue and at the nipple, which indicates problems with differentiation of lesions from healthy tissue, too.

Compared to these results, fluorescence mammography with ICG seems to offer a higher potential for the differentiation of malignant and benign lesions. ICG fluorescence mammograms recorded during the extravascular phase are superior to the intrinsic tissue contrast because (1) carcinomas are visible without background contrast from blood vessels and (2) benign lesions do not show contrast despite enhanced hemoglobin concentration. So far, these results are based on a small number of cases only, and further studies are required to obtain a sufficient data base for evaluating tumor detection and differentiation based on the EPR effect.

4.4 *Monitoring Patient Response to Neoadjuvant Chemotherapy*

The capability of near-infrared spectroscopy to measure functional parameters of carcinomas at known locations within the breast has led to its application for monitoring the response to NAC. This therapy is increasingly used for patients with locally advanced breast cancer to shrink tumor size prior to surgery. NAC has been shown to increase the rate of breast-conserving surgery.[166] Moreover, patients with a pathological complete response to chemotherapy are associated with longer disease-free and overall survival.[167] It is desirable to predict the likely success of NAC as early as possible, preferentially before or right after its start. For this purpose, functional imaging methods seem to be better suited than morphological imaging techniques.[168] Compared to techniques like dynamic contrast-enhanced MRI or PET mammography, NIR spectroscopy is technically less demanding and does not need a contrast agent.

The first application of optical imaging for NAC treatment monitoring was demonstrated at the University of California, Irvine.[169] Meanwhile, several of the instruments discussed in Sec. 3 have been employed in corresponding clinical studies including multimodality imagers. Using the DOSI instrument, Cerussi et al.[170] found that for a 3-month NAC treatment with adriamycin/cytoxan, pathologic complete responders and nonresponders could be distinguished already after the first week of the therapy. At this time point, deoxy-Hb concentration and water concentration had dropped by $27\% \pm 15\%$ and $11\% \pm 15\%$, respectively, for responders, whereas nonresponders did not show any significant changes in these parameters. The differentiation between responders and nonresponders was also obtained when the reduction of HbT was considered instead. Furthermore, the responder group showed a significantly larger tumor-to-normal ratio of oxy-Hb than the nonresponders before NAC. In other words, the carcinomas in the nonresponder group should originally have had a lower StO_2 value compared to the responders. This assumption was then confirmed in a later paper, where a pretreatment StO_2 threshold value of 76.7% was found between the two groups.[171] Another study with the DOSI instrument revealed that pathologic complete responders and partial responders could already be distinguished from nonresponders 1 day after start of the NAC by a characteristic flare in the tumor oxy-Hb concentration. On average, this increase in the responder group amounted to more than 40% of the baseline value.[168]

These investigations caught the interest of a number of groups involved in breast tissue optical spectroscopy. As discussed above, the objective is to discriminate responders from nonresponders as early as possible, ideally before or shortly after the start of chemotherapy. Soliman et al. proposed to consider the amount of deoxy-Hb and the water volume instead of the deoxy-Hb concentration and the water volume fraction when investigating patients that obtained different NAC treatments.[172,173] By taking these quantities for the entire breast, not only for the lesion volume, a differentiation between responders and nonresponders was obtained after the first week of treatment. At this time point, an increase of both quantities was observed for responders, whereas nonresponders showed a decrease. Four weeks after the start of the treatment, separation worked best for the amount of deoxy-Hb in the lesion and not in the whole breast. The investigations were performed with a commercial instrument (SoftScan from ART, Canada) that provides hemoglobin concentration, fractional water volume, lipid fraction as well as scatter power and scatter amplitude values from measurements at four wavelengths between 690 and 830 nm.[173]

A clinical study with the combined optical and ultrasound handheld probe of the University of Connecticut showed for the first time that responders and nonresponders to NAC are characterized by differences in the pretreatment tumor hemoglobin level. Pathologic complete and near-complete responders exhibited significantly higher tumor concentrations in HbT (75.7 ± 18.8 μM) as well as in oxy- and deoxy-Hb than subjects with modest or no response (tumor average HbT of 51 ± 14 μM).[174] Recently, Zhu et al.[175] proposed a prediction model for NAC response combining HbT concentrations with conventional pathologic tumor parameters. Unlike Zhu et al., who utilized absolute values of HbT concentrations, Jiang et al.[176] considered relative baseline values of pretreatment tumor HbT with respect to the contralateral breast. In a clinical study on 19 patients with the combined MR-optical instrument developed at Dartmouth College, these relative values were found to be significantly different between responders and nonresponders. Perfect differentiation was obtained when the percent change in tumor HbT within the first cycle of treatment was taken as criterion, which was similar to a previous observation on seven

patients.[177] In an exploratory single case study, NIR spectroscopy was performed together with DCS using a handheld probe. Hereby, the tumor-to-normal blood flow contrast was significantly increased on day 3 and significantly decreased on day 5 after start of treatment.[178] Recently, investigations have been started with the dynamic dual breast imager developed by NIRx Technologies. Two weeks after start of the NAC, pathological complete responders showed a faster recovery of deoxy-Hb after a short breath hold than partial and nonresponders.[179]

Several studies discussed the time-dependent change of the tumor functional properties over different treatment cycles, in part until the end of NAC.[141,169,172,173,180–182] Pakalniskis et al.[141] reported that tumor HbT decreases significantly during NAC for pathologic complete responders and not for partial responders. A similar trend is visible in the long-term tumor data of Falou et al.[172,173] Schaafsma et al.[182] focused on the investigation of patients with HER2-negative breast cancer, which is associated with decreased angiogenesis resulting in less pronounced differences in HbT between tumor and healthy tissue. The 18 responders in this study showed a statistically significant decrease in oxy-Hb concentration already after the first treatment cycle compared to the four nonresponders. The predictive value for differentiating responders and nonresponders was comparable to DCE-MRI based measurements of tumor volume carried out after the third of six treatment cycles and appeared to outperform DCE-MRI evaluation according to the response evaluation criteria of solid tumors guidelines.[182]

The various investigations have shown that optical imaging is a well suited tool for monitoring the progress during NAC. Functional parameters are highly correlated to the patient's response to treatment. In this scenario, the location of the tumor is known and the original size of the tumor is large, which enables one to determine the functional parameters with high signal-to-noise ratio. On the other hand, there are still many differences in the investigated types of NAC, in patient groups, in measurement protocols, data registration, and analysis that all together hamper the comparison of the results obtained. In particular, different approaches were used to determine the numbers of responders and nonresponders from pathological assessment. Generally, subjects can be divided into pathologic complete responders, partial responders, and nonresponders. Hereby, complete response is typically defined as microscopic evidence that invasive cancer cells had entirely disappeared. In some studies, subjects with a reduction in tumor size of at least 50% were considered as partial responders, otherwise as nonresponders.[168] In other studies, classification of partial responders and nonresponders was based on grading of tumor cellularity.[174,182] In part, the size criteria was combined with the additional demand of a significant decrease in tumor cellularity to classify a subject as (partial) responder.[172,173] The different ways of pathological classification can have considerable influence on the evaluation of the optical monitoring method, e.g., Cerussi et al.[170] mentioned explicitly that their number of responders differed when using either a binary or a tertiary pathologic classification scheme. Furthermore, since a pathological complete response is accepted as important prognostic factor, some investigators evaluated NIR monitoring of NAC by considering only pathologic complete responders as true responders, whereas partial responders and nonresponders were combined in the overall nonresponder group. Other investigators took complete and partial responders into the same group and the remaining nonresponders as the alternative group.

This variety of approaches emphasizes the need for improved consensus, and that care has to be taken when comparing results from various studies available. Furthermore, to achieve clinical translation, joint efforts should be undertaken to impressively demonstrate the advantages of the optical monitoring technique as a contribution to personalized treatment of patients. A first step into this direction is the multicenter clinical trial of DOSI instruments, recently started at five clinical sites.[183] It remains to be seen how early and how reliable breast tissue optical spectroscopy can predict the outcome of NAC, preferentially even for pretreated subjects, with clear potential benefits for patients and cost reduction for the healthcare systems.

4.5 *Assessment of Breast Density and Estimate of Cancer Risk*

Breast density is a measure of the extent of radiodense fibroglandular tissue in the breast.[184] It reflects composition in terms of fat, stromal, and epithelial tissues. As implied by its definition, it is assessed either from the qualitative or quantitative analysis of x-ray mammograms. In the former case, which is still most common in clinical practice, x-ray mammograms are visually inspected by an expert radiologist, and breast density is most often classified through BI-RADS categories:[184] (1) almost entirely fat; (2) scattered fibroglandular densities; (3) heterogeneously dense; and (4) extremely dense. However, the quantitative estimate of breast density is becoming more and more widespread. It is performed analyzing x-ray mammograms with dedicated percentage of dense (fibroglandular) tissue present in the breast.

The importance of the assessment of breast density comes from its identification as a risk factor. Over the years, a large number of studies have investigated breast density, and it is now widely recognized that it is a strong independent risk factor for developing breast cancer. Actually, it is the strongest risk factor, apart from gender and age: it has been observed that risk is two to six times higher in women with dense breasts (BI-RADS category 4) than in women with fatty breasts (BI-RADS category 1).[185] High density also increases significantly the risk of cancer recurrence.[186]

The information on breast density can be useful to identify women that are at high risk and deserve personalized screening/diagnostic paths. Moreover, different from other risk factors, breast density can be modified. Thus, its estimate can help monitoring the effects of interventions that aim at reducing breast density and the related risk. Actually, not only the preventive administration of chemotherapy drugs can reduce breast density but also nonpharmaceutical interventions, like changes in the diet or lifestyle.[187,188] Breast density can also be exploited as an intermediate endpoint in studies on breast cancer etiology. Finally, information on breast density has recently proved useful to predict the pathologic response to neoadjuvant chemo-[189] or endocrine therapy.[190]

As mentioned above, x-ray mammography is the gold standard for the assessment of breast density and the method that is generally applied in clinical practice. This implies that the information on breast density becomes known only at the time of the first mammography, typically at the age of 50.[191] On the contrary, both for monitoring women at high risk and for devising actions to reduce breast density, it would be beneficial to know it earlier in life. MRI has effectively been applied to estimate the amounts of fibroglandular and fat tissue.[192,193] However, high costs, long measurement times, and, in some cases, limited patient acceptance make MRI unsuitable for screening wide

populations. The sensitivity of optical techniques to tissue composition and their general features (relatively inexpensive and simple to operate, well accepted, generating absolute, operator-independent results) makes them potentially interesting candidates as alternative means for the estimate of breast density.

Starting a decade ago, this possibility has been extensively investigated by Lilge and coworkers in Toronto.[116,194] In particular, they have been performing CW transmittance spectroscopy over a broad spectral range (625 to 1060 nm) at four positions (central, medial, distal, and lateral) on both breasts and interpreting transmittance data with principal component analysis. The principal components reflect variations in tissue attenuation (due to both absorption and scattering properties) and, thus, contain information on tissue composition and density. Each spectrum is a weighted average of component spectra, each weighted by a score. Four principal components proved to account for almost the entire tissue variability. Collecting data on more than 200 volunteers, they have shown good correlation between the four scores and percentage mammographic density (assessed using Cumulus,[195] a computer-assisted thresholding software for the analysis of x-ray mammograms).[194]

At Politecnico di Milano, we have applied time-resolved diffuse optical imaging performed at seven wavelengths (635 to 1060 nm) to estimate breast tissue composition and structure of 2018 subjects. In particular, time-domain operation in a wavelength range extending beyond 900 nm allowed not only the assessment of blood parameters (total hemoglobin content and oxygenation level), as typically performed by optical instruments, but also of tissue composition in terms of water, lipid, and collagen. The scattering parameters (amplitude a, i.e., scattering at 600 nm, and power b) were also estimated. The results confirmed strong positive correlation with optically derived water content (and corresponding negative correlation with lipid content), as expected, considering that water strongly absorbs x-rays, while adipose tissue is essentially translucent to x-rays. An optical index based on tissue composition and structure proved suitable to classify noninvasively breast density in agreement with BI-RADS classification performed by an expert radiologist.[196]

Even more interesting, collagen content and scattering slope b increased progressively and significantly with breast density.[196] Some other limited studies also confirmed the positive correlation between scattering parameters and mammographic density.[197–199] The scattering properties, especially the scattering power, are expected to depend on collagen structure in tissue. So, the combination of collagen content and scattering parameters may be used to obtain more comprehensive information on collagen in breast tissue. Collagen is a protein family and a major constituent of connective tissue. Fibrillar collagens are essential in determining stromal architecture [see Figs. 1(b) and 2(b)]. Morphological alterations that can be attributed to changes in collagen content and structure occur in breast stroma not just during invasive tumor growth but also in the preneoplastic phase: alterations of stromal architecture and composition are a well-known aspect of both benign and malignant pathologies, and may play an initial role in breast carcinogenesis.[200–202] The optical assessment of collagen content (and potentially also of collagen structure through scattering parameters) may prove of great interest for the assessment of cancer risk, which is associated to mammographic density. Based on what has been discussed above on the link between collagen and cancer development, it might provide noninvasively a more direct estimate of risk than x-ray mammography, which is more sensitive to water content than to collagen. Recently, very preliminary data have also suggested that collagen might provide independent information on risk with respect to mammographic density.[203] If confirmed, this hypothesis would further increase the interest in optical means for the estimate of cancer risk.

4.6 *Dependence of Breast Tissue Composition and Structure on Demographic Parameters*

Two recent works on the estimate of breast density (see Sec. 4.5) have applied broadband[117] or multiple-wavelength[204] acquisition over an extended spectral range (650 to 1000 nm or wider) on more than 200 subjects. Blackmore et al.[117] studied how blood parameters (HbT and StO_2), water and lipid content, and scattering parameters (amplitude and slope) vary with age and body mass index (BMI) in pre- and postmenopausal women. Taroni et al.[204] estimated tissue composition (water, lipids, and collagen), functional information (blood parameters HbT and StO_2), and information on the microscopic structure of tissue (scattering amplitude a, i.e., scattering coefficient at 600 nm, and power b), investigating the correlation with age, BMI, menopausal status, and use of oral contraceptives. Both studies highlighted how age, BMI, and menopause affect tissue composition, increasing the weight of the adipose fraction at the expense of the fibroglandular fraction. This corresponds to significant decrease in water and collagen content and corresponding increase in lipid content. The total hemoglobin content also decreases, while the trend for oxygen saturation is less clear.

The use of oral contraceptives seems to have opposite effect, corresponding to an increase in the fibroglandular tissue fraction. After age adjustment, the trend is the same, but the difference between users of oral contraceptives and nonusers are no longer statistically significant or only close to significance. However, it should be taken into account that complete information (e.g., duration of use) was missing for several subjects, thus further studies are needed to draw definite conclusions. In particular, data referring to the effects of the menopausal status are reported in Table 3. In one case, tissue composition is estimated as relative percentage values and in the other one as absolute concentrations. However, the trends with menopause are very similar for all measured parameters, except for the scattering power, which showed a significant decrease in the study by Taroni et al., while it did not vary significantly in the study of Blackmore et al.

Over the years, the DOSI system developed at the University of California, Irvine,[51] has also provided pieces of information on breast tissue composition affected by menopausal status. A recent example is represented by the study performed to monitor changes in tissue composition in 28 breast cancer patients undergoing neoadjuvant chemotherapy (see Sec. 4.4). In that case, baseline (pretherapy) water and lipid content in breast tissue was shown to depend markedly on the menopausal status, in agreement with what described above, and also to correlate with fibroglandular density assessed by MRI.

It is important to stress that optically derived data reported in the literature on tissue composition and structure and their changes are fully consistent with the present knowledge on breast physiology, which has often been obtained through *ex vivo* analyses or studies performed with invasive or more complex and expensive approaches than optical ones (e.g., x-ray mammography and MRI, respectively). The good correspondence between optically derived information and medical knowledge, combined with well-known and already mentioned advantages of optical means (including noninvasiveness, limited costs, good patient acceptance), indicates that optical spectroscopy

Table 3 Dependence of tissue composition and structure (mean ± SD) on menopausal status (N = number of subjects, N.A. = not available).

References	Menopausal status	Water (%)	Lipid (%)	Collagen (%)	HbT (μM)	StO_2 (%)	a (cm^{-1})	b (—)
Blackmore et al.[117]	Pre- ($N = 95$)	21.3 ± 7.2	61.5 ± 10.2	N.A.	15.7 ± 4.8	70.5 ± 7.6	14.6 ± 3.4	0.35 ± 0.31
	Post- ($N = 107$)	18.2 ± 5.9	68.3 ± 9.0	N.A.	12.4 ± 4.7	68.5 ± 8.0	12.9 ± 2.9	0.38 ± 0.26
		Water (mg/cm^3)	Lipid (mg/cm^3)	Collagen (mg/cm^3)	HbT (μM)	StO_2 (%)	a (cm^{-1})	b (—)
Taroni et al.[204]	Pre- ($N = 93$)	263.1 ± 148.4	598.3 ± 133.5	98.73 ± 43.0	13.6 ± 4.1	86.8 ± 9.6	14.9 ± 2.6	0.70 ± 0.27
	Post- ($N = 102$)	127.9 ± 86.3	730.0 ± 111.2	64.3 ± 34.1	10.4 ± 3.2	84.9 ± 9.1	12.4 ± 2.5	0.53 ± 0.24

could take on an effective role to investigate breast physiology *in vivo* and monitor changes in breast tissue through longitudinal studies (e.g., during chemotherapy or with age).

5 Emerging Fields in the Realm of Breast Imaging and Spectroscopy

5.1 *Photoacoustic Mammography*

PI (or optoacoustic imaging) of the breast combines the high contrast arising from light absorption in tissue with the high spatial resolution associated with ultrasound detection. The local absorption of light by tissue chromophores or contrast agents leads to thermoelastic expansion of the tissue and to the formation of pressure waves. From the detected ultrasound signals, the location of the absorbers can be estimated with superior spatial resolution compared to diffuse optical imaging. At present, photoacoustic mammography relies essentially on blood contrast and, hence, carcinomas and benign lesions can be detected due to the increase in local deoxy-, oxy-, and total hemoglobin concentration associated with angiogenesis of these lesions. Although a laser optoacoustic imaging system for the breast was proposed by Oraevsky et al.[205] as early as in 1996, only more recently clinical systems have been applied in exploratory studies. Here, we will shortly report on the main features of breast PI prototypes. An extensive survey has recently been performed by Menke.[206]

The most recent clinical studies have been performed using the Twente Photoacoustic Mammograph. In the latest version of this prototype,[207,208] the patient is lying in prone position with the breast pending through an aperture and mildly compressed between a glass window and an ultrasound detector array containing 588 elements. The breast is illuminated through the glass plate by a pulsed laser at 1064 nm with 10-ns pulses at a repetition rate of 10 Hz using a beam diameter of ~70 mm. Information from x-ray mammograms and ultrasound images are used to define a region of interest on the breast, which is then scanned by the laser beam. Depending on penetration depth, the lateral resolution, and the axial resolution range from 2.3 to 3.9 mm and from 2.5 to 3.3 mm, respectively.[207–209]

The case studies performed over a period of 8 years on a total of 23 patients with breast tumors have shown tumors with high imaging contrast. In the most recent study on 11 patients,[207] with MRI data available, excellent correspondence in lesion localization was found between PI and MRI images, together with a good to reasonable correlation in lesion shape and appearance. Moreover, it is important to notice that PI images were not affected by the breast density. In patients with cysts (six cases), the lesion was visible with high contrast only at the front and/or at the back of the cyst where impedance changes occur, leading to possible misdiagnosis since malignancies can also appear as one or multiple confined contrast areas.[208,210]

The Canon prototype presented a configuration similar to that of the Twente mammograph with respect to patient position and breast compression geometry.[211] The illumination system was different and relied on two sources to provide forward and backward illumination with respect to the 345 element array transducer. The forward and backward laser pulses could be applied simultaneously to maximize optical fluence in the region of interest or alternately to evaluate forward and backward images separately. The laser source was a tunable Ti: Sapphire laser (15-ns pulses at 10-Hz repetition rate). The lateral resolution was 2 to 3 mm. Clinical data were obtained from 26 patients with breast cancer. Images were acquired at both 756- and 797-nm wavelengths to evaluate total hemoglobin content and oxygen saturation. The tumors were correctly detected in 20 cases. The PI images showed high contrast related to the higher hemoglobin content, with tumor margins less defined as compared to MRI images.

The original laser optoacoustic imaging system (LOIS) proposed by Oraevsky et al.[212] was further developed to perform optoacoustic tomography (LOIS-64).[213] With the patient in prone position, the uncompressed breast was suspended through a circular hole in a probe cup. An arc-shaped 64 elements ultrasound transducer array was rotated around the breast to acquire a set of 2-D images each with a depth resolution of 0.5 mm. The expanded laser beam was provided by a Q-switched Alexandrite laser emitting at 757 nm, with pulse duration of 75 ns at a repetition rate of 10 Hz. In the clinical study performed on 27 patients, the LOIS-64 prototype revealed 18 out of 20 histologically proven malignant lesions and 4 out of 8 benign lesions. In all cases detected, the tumor area presented high contrast attributed to high tumor vascularization.

Although not yet tested on breast cancer patients, the OptoSonics 512 prototype presents interesting features.[214] With the patient in prone position, the breast is placed in a spherical cup, designed to be optically transparent and with an acoustic transmittance larger than 70% at 2 MHz. This cup is positioned in a hemispherical bowl equipped with 512 ultrasound transducers (3 mm × 3 mm size). The pendant breast being pushed toward the chest wall by the cup is illuminated from below by an Alexandrite laser at 756 nm with a pulse repetition rate of 10 Hz. The system was tested on four healthy volunteers with breast thickness between 2.3 and 4 cm. The reconstructed images clearly showed the breast vasculature with

submillimeter resolution. The estimated spatial resolution of the system is 0.42 mm and, based on the phantom study, the authors expect to be able to image tissues as thick as 5.3 cm.

The features of the presently available clinical prototypes illustrate the potential of the photoacoustic approach. Several problems, however, are still open ranging from technical aspects (e.g., detectors sensitivity, field of view), the methodology of the reconstruction algorithms, and the biological basis for discriminating malignant from benign lesions. Clearly, larger clinical studies on both malignant and benign lesions are needed. As for diffuse optical imaging and tomography, improvements might come from multispectral operation and/or integration with other diagnostic modalities, as, e.g., diffuse optical imaging/tomography and ultrasound imaging, to combine information on tissue properties from different approaches. Examples of these integrated modalities are already present in the literature with tests on phantoms or *ex vivo* specimens.[215–217]

A further proposed approach is related to the development of handheld photoacoustic devices, which have the advantage to be simple, portable, and can be easily integrated in an ultrasound probe.[218–220] As for other diagnostic modalities, improvements might come from molecular imaging. In fact, suitable chromophores might enhance the sensitivity and specificity of the diagnostic images, which presently rely essentially on blood contrast.[221] Similarly, in hybrid ultrasound and photoacoustic systems, ultrasonic contrast agents can be useful for both modalities.

5.2 *Long Wavelength Broadband Spectroscopy*

Up to now, multiple-wavelength and broadband imaging and spectroscopy of the breast have been performed at most up to 1000 to 1100 nm. However, it is interesting to observe that the spectral range available for tissue spectroscopy is extending toward longer wavelengths, up to 2 μm and beyond. The total attenuation coefficient was measured *ex vivo* on thin (200 μm) slices of breast tissue (healthy and cancerous) between 400 and 2500 nm, showing that in the second (1100 to 1350 nm) and even more in the third (1600 to 1850 nm) NIR optical window, deeper light penetration can be achieved compared to the conventional first NIR window (650 to 950 nm). Moreover, in the second and third windows, the scattering becomes progressively less than in the first window, and light attenuation is dominated by tissue chromophore absorption, suggesting the possibility to perform imaging with reduced blurring with respect to what typically observed in diffuse optical images.[222] Moreover, it has been reported that fitting tissue composition and scattering parameters over an extended spectral range (500 to 1600 nm instead of 500 to 1000 nm), which includes more spectral features, can significantly improve the results (i.e., the confidence level on the estimate of water and lipid fractions can improve by a factor of 4).[223] Recent advances in laser sources, especially supercontinuum fiber sources, and detectors have made it possible to develop portable systems and apply them to perform diffuse optical spectroscopy in clinical settings at least up to 1350 nm,[224] suggesting that results on *in vivo* breast studies beyond 1000 to 1100 nm will soon become available.

6 Conclusions

During the last 20 years, tremendous amount of work has been carried out on *in vivo* optical imaging of the female breast. Starting from attempts to obtain high-contrast images of breast carcinomas by a noninvasive and comparably cheap method, the focus of research moved more and more to the development of methods suited to quantitatively measure the functional parameters of breast tissue and to understand the origin of contrast in near-infrared images of diseased as well as healthy breast tissue. The present knowledge on functional and scattering properties shows why the initial idea to find carcinomas and to distinguish them from benign lesions due to contrast in hemoglobin concentration and oxygen saturation was not successful. Locally increased hemoglobin concentration is not only a feature of cancer but also of many benign tissue alterations, and oxygen saturation of carcinomas is not suited for their differentiation, at least if no detailed information on perfusion is available. Improved spectral resolution has shown that water, lipid, and collagen content and also scattering properties are different between cancer and healthy breast tissue. In the future, long wavelength broadband spectroscopy extending tissue optical spectroscopy further into the infrared spectral range offers to more accurately determine concentrations of the tissue constituents. Furthermore, DCS has shown that the blood flow index is another promising quantity to differentiate carcinomas from healthy tissue, in particular, when a detailed physical model for the loss of correlation becomes available.

Currently, sensitivity and specificity of optical mammography are likely too low for its application as a screening tool. More importantly, the poor spatial resolution of diffuse optical imaging prevents early detection of breast cancer, which is a main aim of screening. Although PI may overcome this limitation, it is an open question, whether the stringent requirements for screening of high sensitivity, high specificity, and high patient throughput can be met by this modality. Instead, the unique capabilities of optical breast imaging offer high potential for its use as an adjunct modality in diagnostic mammography and as a tool for monitoring cancer therapy. Hereby, known lesions in the breast are characterized by their functional parameters. With respect to diagnosis, this additional information could possibly help to reduce the number of biopsies that are necessary for assessing malignancy of suspicious lesions and to avoid frequent false positive results. Several clinical studies have shown improved sensitivity and specificity of conventional imaging modalities, when known lesions are additionally characterized by functional parameters from near-infrared spectroscopy. Currently, the power of the various functional properties, including scattering parameters, is differently assessed by various research groups, which is evident, e.g., from the various proposed tissue optical indices. Future work should aim at a more comparable database to select the properties with the highest potential for differentiation, and to identify preferred approaches of tumor assessment for specific subgroups of patients.

Besides the intrinsic tissue contrast, optical contrast agents are of high potential for the differentiation of suspicious lesions. The EPR effect using plasma proteins labeled with the fluorescent marker ICG offers a unique method to assess the leakiness of the tumor vasculature. Quantitative results on ICG extravasation are also of interest for intraoperative fluorescence detection of tumor margins using ICG, an approach starting to play a role in breast-conserving cancer surgery. Furthermore, the detection of weak fluorescence signals demonstrated with the available contrast agents indicates that other fluorescent molecular agents could be detected, once they become available. Depending on the power of such agents, new applications of fluorescence breast imaging could arise.

Looking toward the different research activities associated with optical breast imaging, monitoring the patient's response to NAC seems to be closest to clinical translation. Available data show strong evidence that early evaluation of the response to the treatment should allow one to predict success or failure of NAC. Another potential application of near-infrared spectroscopy of the breast is the evaluation of breast density as a risk factor for developing cancer. Although totally different with respect to target groups, both applications offer ways toward a personalized therapy using optical breast imaging.

Photoacoustic mammography offers the advantage to image the breast with superior spatial resolution compared to diffuse optical imaging. In particular, vascular structures can be resolved even deeply inside the breast with higher resolution as can be achieved with diffuse optical mammography. At present, potential of photoacoustic mammography for detection and characterization of breast carcinomas and benign lesions has not been evaluated yet, and image contrast is based on the same absorbing tissue volumes, chromophores, or contrast agents that are used in diffuse optical imaging. Tissue scattering properties and sensitive fluorescence detection are not accessible by this method.

In order to better understand the origin of host-tumor contrast in near-infrared breast images or tissue spectra, advanced tissue models are needed.[225,226] The remodeling of vasculature, lymphatics, ECM, and the invasion of cells of different origin caused by the presence of carcinoma represent complex, in part chaotic biological processes that are presently being unraveled by tumor biology. Such processes alter, e.g., vascular morphology, biochemical composition, and mechanical as well as scattering properties of the ECM. Furthermore static and dynamical physical measures, such as perfusion, interstitial flow, as well as solid and interstitial fluid pressure, are affected. Such changes bear on the quantities that can be measured by optical mammography and breast tissue spectroscopy. To fully exploit the information contained in clinical data, improved tissue models are needed, which in turn can be further improved by including clinical results. Such models will contribute to a better understanding of physical processes associated with tumor pathophysiology and, eventually, will add to better treatment.

References

1. N. Howlader et al., Eds., *SEER Cancer Statistics Review, 1975—2012*, National Cancer Institute, Bethesda, Maryland (2015).
2. P. D. Sasieni et al., "What is the lifetime risk of developing cancer?: the effect of adjusting for multiple primaries," *Br. J. Cancer* **105**(3), 460–465 (2011).
3. E. D. Pisano et al., "Diagnostic performance of digital versus film mammography for breast-cancer screening," *N. Engl. J. Med.* **353**(17), 1773–1783 (2005).
4. N. Hylton, "Magnetic resonance imaging of the breast: opportunities to improve breast cancer management," *J. Clin. Oncol.* **23**(8), 1678–1684 (2005).
5. S. J. Lord et al., "A systematic review of the effectiveness of magnetic resonance imaging (MRI) as an addition to mammography and ultrasound in screening young women at high risk of breast cancer," *Eur. J. Cancer* **43**(13), 1905–1917 (2007).
6. C. L. Christiansen, "Predicting the cumulative risk of false-positive mammograms," *J. Natl. Cancer Inst.* **92**(20), 1657–1666 (2000).
7. R. A. Hubbard et al., "Cumulative probability of false-positive recall or biopsy recommendation after 10 years of screening mammography: a cohort study," *Ann. Intern. Med.* **155**(8), 481–492 (2011).
8. R. McLaughlin and N. Hylton, "MRI in breast cancer therapy monitoring," *NMR Biomed.* **24**(6), 712–720 (2011).
9. D. T. Butcher, T. Alliston, and V. M. Weaver, "A tense situation: forcing tumour progression," *Nat. Rev. Cancer*," **9**(2), 108–122 (2009).
10. M. Egeblad, E. S. Nakasone, and Z. Werb, "Tumors as organs: complex tissues that interface with the entire organism," *Dev. Cell* **18**(6), 884–901 (2010).
11. C. Frantz, K. M. Stewart, and V. M. Weaver, "The extracellular matrix at a glance," *J. Cell Sci.* **123**(Pt 24), 4195–4200 (2010).
12. T. R. Cox and J. T. Erler, "Remodeling and homeostasis of the extracellular matrix: implications for fibrotic diseases and cancer," *Dis. Model. Mech.* **4**(2), 165–178 (2011).
13. R. K. Jain and D. Duda, "Vascular and interstitial biology of tumors," in *Abeloff's Clinical Oncology*, 4th ed., M. Abeloff et al., Eds., pp. 105–124, Churchill Livingstone Elsevier, Philadelphia (2008).
14. J. A. Nagy et al., "Why are tumour blood vessels abnormal and why is it important to know?," *Br. J. Cancer* **100**(6), 865–869 (2009).
15. J. Holash et al., "Vessel cooption, regression, and growth in tumors mediated by angiopoietins and VEGF," *Science* **284**(5422), 1994–1998 (1999).
16. G. D. Yancopoulos et al., "Vascular-specific growth factors and blood vessel formation," *Nature* **407**(6801), 242–248 (2000).
17. J. Folkman, "Tumor angiogenesis: therapeutic implications," *N. Engl. J. Med.* **285**(21), 1182–1186 (1971).
18. P. Carmeliet and R. K. Jain, "Angiogenesis in cancer and other diseases," *Nature* **407**(6801), 249–257 (2000).
19. H. G. Augustin, G. Y. Koh, G. Thurston, and K. Alitalo, "Control of vascular morphogenesis and homeostasis through the angiopoietin-Tie system," *Nat. Rev. Mol. Cell Biol.* **10**(3), 165–177 (2009).
20. R. H. Adams and K. Alitalo, "Molecular regulation of angiogenesis and lymphangiogenesis," *Nat. Rev. Mol. Cell Biol.* **8**(6), 464–478 (2007).
21. R. Erber et al., "EphB4 controls blood vascular morphogenesis during postnatal angiogenesis," *EMBO J.* **25**(3), 628–641 (2006).
22. S. M. Weis and D. A. Cheresh, "Tumor angiogenesis: molecular pathways and therapeutic targets," *Nat. Med.* **17**(11), 1359–1370 (2011).
23. D. Neri and R. Bicknell, "Tumour vascular targeting," *Nat. Rev. Cancer* **5**(6), 436–446 (2005).
24. M. W. Dewhirst, Y. Cao, and B. Moeller, "Cycling hypoxia and free radicals regulate angiogenesis and radiotherapy response," *Nat. Rev. Cancer* **8**(6), 425–437 (2008).
25. V. P. Chauhan et al., "Delivery of molecular and nanoscale medicine to tumors: transport barriers and strategies," *Annu. Rev. Chem. Biomol. Eng.* **2**, 281–298 (2011).
26. T. P. Padera et al., "Pathology: cancer cells compress intratumour vessels," *Nature* **427**(6976), 695 (2004).
27. T. Stylianopoulos et al., "Causes, consequences, and remedies for growth-induced solid stress in murine and human tumors," *Proc. Natl. Acad. Sci. U. S. A.* **109**(38), 15101–15108 (2012).
28. J. M. Brown and W. R. Wilson, "Exploiting tumour hypoxia in cancer treatment," *Nat. Rev. Cancer* **4**(6), 437–447 (2004).
29. J. M. Brown, "The hypoxic cell," *Cancer Res.* **59**(23), 5863–5870 (1999).
30. H. Maeda, G. Y. Bharate, and J. Daruwalla, "Polymeric drugs for efficient tumor-targeted drug delivery based on EPR-effect," *Eur. J. Pharm. Biopharm.* **71**(3), 409–419 (2009).
31. Y. Matsumura and H. Maeda, "A new concept for macromolecular therapeutics in cancer chemotherapy: mechanism of tumoritropic accumulation of proteins and the antitumor agent smancs," *Cancer Res.* **46**(12 Pt 1), 6387–6392 (1986).
32. D. M. Gilkes, G. L. Semenza, and D. Wirtz, "Hypoxia and the extracellular matrix: drivers of tumour metastasis," *Nat. Rev. Cancer* **14**(6), 430–439 (2014).
33. M. Cutler, "Transillumination as an aid in the diagnosis of breast lesions," *Surg. Gynecol. Obstet.* **48**, 721–729 (1929).
34. M. Cutler, "Transillumination of the breast," *Ann. Surg.* **93**(1), 223–234 (1931).
35. C. Gros, Y. Quenneville, and Y. Hummel, "Diaphanologie mammaire," *J. Radiol. Electrol. Med. Nucl.* **53**(4), 297–306 (1972).
36. D. J. Watmough, "Diaphanography: mechanism responsible for the images," *Acta Radiol. Oncol.* **21**(1), 11–15 (1982).
37. V. Marshall, D. C. Williams, and K. D. Smith, "Diaphanography as a means of detecting breast cancer," *Radiology* **150**(2), 339–343 (1984).
38. S. Ertefai, "Spectral transmittance and contrast in breast diaphanography," *Med. Phys.* **12**(4), 393 (1985).
39. A. E. Profio, "Scientific basis of breast diaphanography," *Med. Phys.* **16**(1), 60 (1989).
40. G. E. Geslien, J. R. Fisher, and C. DeLaney, "Transillumination in breast cancer detection: screening failures and potential," *Am. J. Roentgenol.* **144**(3), 619–622 (1985).

41. J. J. Gisvold et al., "Comparison of mammography and transillumination light scanning in the detection of breast lesions," *Am. J. Roentgenol.* **147**(1), 191–194 (1986).
42. B. Monsees, J. M. Destouet, and W. G. Totty, "Light scanning versus mammography in breast cancer detection," *Radiology* **163**(2), 463–465 (1987).
43. A. Alveryd et al., "Lightscanning versus mammography for the detection of breast cancer in screening and clinical practice. A Swedish multicenter study," *Cancer* **65**(8), 1671–1677 (1990).
44. R. L. P. van Veen et al., "Intraoperatively assessed optical properties of malignant and healthy breast tissue used to determine the optimum wavelength of contrast for optical mammography," *J. Biomed. Opt.* **9**(6), 1129–1136 (2004).
45. A. Corlu et al., "Uniqueness and wavelength optimization in continuous-wave multispectral diffuse optical tomography," *Opt. Lett.* **28**(23), 2339 (2003).
46. D. Grosenick et al., "A multichannel time-domain scanning fluorescence mammograph: performance assessment and first *in vivo* results," *Rev. Sci. Instrum.* **82**(2), 024302 (2011).
47. R. Choe et al., "Differentiation of benign and malignant breast tumors by *in-vivo* three-dimensional parallel-plate diffuse optical tomography," *J. Biomed. Opt.* **14**(2), 024020 (2009).
48. S. B. Colak et al., "Clinical optical tomography and NIR spectroscopy for breast cancer detection," *IEEE J. Sel. Top. Quantum Electron.* **5**(4), 1143–1158 (1999).
49. L. C. Enfield et al., "Three-dimensional time-resolved optical mammography of the uncompressed breast," *Appl. Opt.* **46**(17), 3628–3638 (2007).
50. B. W. W. Pogue et al., "Characterization of hemoglobin, water, and NIR scattering in breast tissue: analysis of intersubject variability and menstrual cycle changes," *J. Biomed. Opt.* **9**(3), 541–552 (2004).
51. T. D. O'Sullivan et al., "Diffuse optical imaging using spatially and temporally modulated light," *J. Biomed. Opt.* **17**(7), 071311 (2012).
52. L. Götz et al., "Optische mammographie an präoperativen patientinnen," *Aktuelle Radiol.* **8**(1), 31–33 (1998).
53. K. T. Moesta et al., "Contrast features of breast cancer in frequency-domain laser scanning mammography," *J. Biomed. Opt.* **3**(2), 129–136 (1998).
54. D. Grosenick et al., "Development of a time-domain optical mammograph and first *in vivo* applications," *Appl. Opt.* **38**(13), 2927 (1999).
55. P. Taroni et al., "Clinical trial of time-resolved scanning optical mammography at 4 wavelengths between 683 and 975 nm," *J. Biomed. Opt.* **9**(3), 464–473 (2004).
56. Y. Yu et al., "Near-infrared spectral imaging of the female breast for quantitative oximetry in optical mammography," *Appl. Opt.* **48**(10), D225–D235 (2009).
57. J. M. Kainerstorfer et al., "Depth discrimination in diffuse optical transmission imaging by planar scanning off-axis fibers: initial applications to optical mammography," *PLoS One* **8**(3), e58510 (2013).
58. T. Dierkes et al., "Reconstruction of optical properties of phantom and breast lesion in vivo from paraxial scanning data," *Phys. Med. Biol.* **50**(11), 2519–2542 (2005).
59. R. Ziegler et al., "Nonlinear reconstruction of absorption and fluorescence contrast from measured diffuse transmittance and reflectance of a compressed-breast-simulating phantom," *Appl. Opt.* **48**(24), 4651 (2009).
60. A. Corlu et al., "Three-dimensional *in vivo* fluorescence diffuse optical tomography of breast cancer in humans," *Opt. Express* **15**(11), 6696–6716 (2007).
61. X. Intes, "Time-domain optical mammography SoftScan: initial results," *Acad. Radiol.* **12**(8), 934–947 (2005).
62. A. Hagen et al., "Development of a multi-channel time-domain fluorescence mammograph," *Proc. SPIE* **6434**, 64340Z (2007).
63. A. Athanasiou et al., "Dynamic optical breast imaging: a new technique to visualise breast vessels: comparison with breast MRI and preliminary results," *Eur. J. Radiol.* **54**(1), 72–79 (2005).
64. S. M. W. Y. van de Ven et al., "A novel fluorescent imaging agent for diffuse optical tomography of the breast: first clinical experience in patients," *Mol. Imaging Biol.* **12**(3), 343–348 (2010).
65. J. Wang et al., "*In vivo* quantitative imaging of normal and cancerous breast tissue using broadband diffuse optical tomography," *Med. Phys.* **37**(7), 3715 (2010).
66. C. H. Schmitz et al., "Design and implementation of dynamic near-infrared optical tomographic imaging instrumentation for simultaneous dual-breast measurements," *Appl. Opt.* **44**(11), 2140–2153 (2005).
67. P. Schneider et al., "Fast 3D near-infrared breast imaging using indocyanine green for detection and characterization of breast lesions," *Rofo* **183**(10), 956–963 (2011).
68. R. J. Grable, D. Rohler, and S. Kla, "Optical tomography breast imaging," *Proc. SPIE* **2979**, 197–210 (1997).
69. D. Floery et al., "Characterization of benign and malignant breast lesions with computed tomography laser mammography (CTLM)," *Invest. Radiol.* **40**(6), 328–335 (2005).
70. R. Ziegler et al., "Investigation of detection limits for diffuse optical tomography systems: I. Theory and experiment," *Phys. Med. Biol.* **54**(2), 399–412 (2009).
71. R. Ziegler et al., "Investigation of detection limits for diffuse optical tomography systems: II. Analysis of slab and cup geometry for breast imaging," *Phys. Med. Biol.* **54**(2), 413–431 (2009).
72. A. E. Cerussi et al., "*In vivo* absorption, scattering, and physiologic properties of 58 malignant breast tumors determined by broadband diffuse optical spectroscopy," *J. Biomed. Opt.* **11**(4), 044005 (2006).
73. A. A. Leproux et al., "Assessing tumor contrast in radiographically dense breast tissue using diffuse optical spectroscopic imaging (DOSI)," *Breast Cancer Res.* **15**(5), R89 (2013).
74. B. Chance et al., "Breast cancer detection based on incremental biochemical and physiological properties of breast cancers: a six-year, two-site study," *Acad. Radiol.* **12**(8), 925–933 (2005).
75. R. X. Xu et al., "Development of a handheld near-infrared imager for dynamic characterization of *in vivo* biological tissue systems," *Appl. Opt.* **46**(30), 7442 (2007).
76. S. J. Erickson and A. Godavarty, "Hand-held based near-infrared optical imaging devices: a review," *Med. Eng. Phys.* **31**(5), 495–509 (2009).
77. Q. Zhu et al., "Ultrasound-guided optical tomographic imaging of malignant and benign breast lesions: initial clinical results of 19 cases," *Neoplasia* **5**(5), 379–388 (2003).
78. Q. Zhu, "Optical tomography with ultrasound localization: initial clinical results and technical challenges," *Technol. Cancer Res. Treat.* **4**(3), 235–244 (2005).
79. V. Ntziachristos and X. H. Ma, "Time-correlated single photon counting imager for simultaneous magnetic resonance and near-infrared mammography," *Rev. Sci. Instrum.* **69**(12), 4221 (1998).
80. V. Ntziachristos et al., "Concurrent MRI and diffuse optical tomography of breast after indocyanine green enhancement," *Proc. Natl. Acad. Sci. U. S. A.* **97**(6), 2767–2772 (2000).
81. V. Ntziachristos et al., "MRI-guided diffuse optical spectroscopy of malignant and benign breast lesions," *Neoplasia* **4**(4), 347–354 (2002).
82. S. Srinivasan et al., "Image guided near-infrared spectroscopy of breast tissue *in vivo* using boundary element method," *J. Biomed. Opt.* **15**(6), 061703 (2010).
83. C. M. Carpenter et al., "MR water quantitative priors improves the accuracy of optical breast imaging," *IEEE Trans. Med. Imaging* **30**(1), 159–168 (2011).
84. Q. Fang et al., "Combined optical imaging and mammography of the healthy breast: optical contrast derived from breast structure and compression," *IEEE Trans. Med. Imaging* **28**(1), 30–42 (2009).
85. H. Rinneberg et al., "Detection and characterization of breast tumours by time-domain scanning optical mammography," *Opto-Electron. Rev.* **16**(2), 147–162 (2008).
86. G. Quarto et al., "Estimate of tissue composition in malignant and benign breast lesions by time-domain optical mammography," *Biomed. Opt. Express* **5**(10), 3684–3698 (2014).
87. P. G. Anderson et al., "Broadband optical mammography: chromophore concentration and hemoglobin saturation contrast in breast cancer," *PLoS One* **10**(3), e0117322 (2015).
88. Q. Fang et al., "Combined optical and X-ray tomosynthesis breast imaging," *Radiology* **258**(1), 89–97 (2011).
89. S. M. W. Y. van de Ven et al., "Diffuse optical tomography of the breast: preliminary findings of a new prototype and comparison with magnetic resonance imaging," *Eur. Radiol.* **19**(5), 1108–1113 (2009).
90. A. H. Gandjbakhche et al., "Time-dependent contrast functions for quantitative imaging in time-resolved transillumination experiments," *Appl. Opt.* **37**(10), 1973 (1998).
91. V. E. Pera et al., "Spatial second-derivative image processing: an application to optical mammography to enhance the detection of breast tumors," *J. Biomed. Opt.* **8**(3), 517–524 (2003).

92. J. R. Mourant et al., "Predictions and measurements of scattering and absorption over broad wavelength ranges in tissue phantoms," *Appl. Opt.* **36**(4), 949 (1997).
93. A. M. Nilsson et al., "Changes in spectral shape of tissue optical properties in conjunction with laser-induced thermotherapy," *Appl. Opt.* **37**(7), 1256–1267 (1998).
94. P. Taroni et al., "Seven-wavelength time-resolved optical mammography extending beyond 1000 nm for breast collagen quantification," *Opt. Express* **17**(18), 15932–15946 (2009).
95. E. L. Heffer et al., "Near-infrared imaging of the human breast: complementing hemoglobin concentration maps with oxygenation images," *J. Biomed. Opt.* **9**(6), 1152–1160 (2004).
96. D. Grosenick et al., "Time-domain optical mammography: initial clinical results on detection and characterization of breast tumors," *Appl. Opt.* **42**(16), 3170–3186 (2003).
97. S. Fantini et al., "Frequency-domain optical mammography: edge effect corrections," *Med. Phys.* **23**(1), 149–157 (1996).
98. F. Bevilacqua et al., "Broadband absorption spectroscopy in turbid media by combined frequency-domain and steady-state methods," *Appl. Opt.* **39**(34), 6498–6507 (2000).
99. D. Grosenick et al., "Concentration and oxygen saturation of haemoglobin of 50 breast tumours determined by time-domain optical mammography," *Phys. Med. Biol.* **49**(7), 1165–1181 (2004).
100. V. Chernomordik et al., "Quantification of optical properties of a breast tumor using random walk theory," *J. Biomed. Opt.* **7**(1), 80–87 (2002).
101. B. Wassermann et al., "*In-vivo* tissue optical properties derived by linear perturbation theory for edge-corrected time-domain mammograms," *Opt. Express* **13**(21), 8571 (2005).
102. A. Torricelli et al., "Use of a nonlinear perturbation approach for *in vivo* breast lesion characterization by multiwavelength time-resolved optical mammography," *Opt. Express* **11**(8), 853–867 (2003).
103. D. Grosenick et al., "Evaluation of higher-order time-domain perturbation theory of photon diffusion on breast-equivalent phantoms and optical mammograms," *Phys. Rev. E* **76**(6), 061908 (2007).
104. H. Dehghani et al., "Multiwavelength three-dimensional near-infrared tomography of the breast: initial simulation, phantom, and clinical results," *Appl. Opt.* **42**(1), 135–145 (2003).
105. S. Srinivasan et al., "Spectrally constrained chromophore and scattering near-infrared tomography provides quantitative and robust reconstruction," *Appl. Opt.* **44**(10), 1858 (2005).
106. J. P. Culver et al., "Three-dimensional diffuse optical tomography in the parallel plane transmission geometry: evaluation of a hybrid frequency domain/continuous wave clinical system for breast imaging," *Med. Phys.* **30**(2), 235–247 (2003).
107. A. Corlu et al., "Diffuse optical tomography with spectral constraints and wavelength optimization," *Appl. Opt.* **44**(11), 2082–2093 (2005).
108. S. R. Arridge, "Optical tomography in medical imaging," *Inverse Probl.* **15**(2), R41–R93 (1999).
109. B. Brooksby et al., "Imaging breast adipose and fibroglandular tissue molecular signatures by using hybrid MRI-guided near-infrared spectral tomography," *Proc. Natl. Acad. Sci. U. S. A.* **103**(23), 8828–8833 (2006).
110. L. Zhang et al., "Direct regularization from co-registered anatomical images for MRI-guided near-infrared spectral tomographic image reconstruction," *Biomed. Opt. Express* **6**(9), 3618–3630 (2015).
111. A. Li et al., "Tomographic optical breast imaging guided by three-dimensional mammography," *Appl. Opt.* **42**(25), 5181 (2003).
112. Q. Fang et al., "Compositional-prior-guided image reconstruction algorithm for multi-modality imaging," *Biomed. Opt. Express* **1**(1), 223–235 (2010).
113. B. Deng et al., "Characterizing breast lesions through robust multimodal data fusion using independent diffuse optical and x-ray breast imaging," *J. Biomed. Opt.* **20**(8), 080502 (2015).
114. Q. Zhu, N. Chen, and S. H. Kurtzman, "Imaging tumor angiogenesis by use of combined near-infrared diffusive light and ultrasound," *Opt. Lett.* **28**(5), 337–339 (2003).
115. Y. Xu and Q. Zhu, "Estimation and imaging of breast lesions using a two-layer tissue structure by ultrasound-guided optical tomography," *J. Biomed. Opt.* **20**(6), 066002 (2015).
116. M. K. Simick et al., "Non-ionizing near-infrared radiation transillumination spectroscopy for breast tissue density and assessment of breast cancer risk," *J. Biomed. Opt.* **9**(4), 794–803 (2004).
117. K. M. Blackmore et al., "The association between breast tissue optical content and mammographic density in pre- and post-menopausal women," *PLoS One* **10**(1), e0115851 (2015).
118. A. Pifferi et al., "Fully automated time domain spectrometer for the absorption and scattering characterization of diffusive media," *Rev. Sci. Instrum.* **78**(5), 053103 (2007).
119. P. Taroni et al., "Intra-subject spatial changes in the optical properties of the female breast: a preliminary two-subject study," *Med. Laser Appl.* **25**(3), 138–146 (2010).
120. A. Pifferi et al., "Spectroscopic time-resolved diffuse reflectance and transmittance measurements of the female breast at different interfiber distances," *J. Biomed. Opt.* **9**(6), 1143–1151 (2004).
121. R. Cubeddu et al., "Effects of the menstrual cycle on the red and near-infrared optical properties of the human breast," *Photochem. Photobiol.* **72**(3), 383 (2000).
122. T. Durduran et al., "Diffuse optics for tissue monitoring and tomography," *Reports Prog. Phys.* **73**(7), 076701 (2010).
123. U. Sunar et al., "Noninvasive diffuse optical measurement of blood flow and blood oxygenation for monitoring radiation therapy in patients with head and neck tumors: a pilot study," *J. Biomed. Opt.* **11**(6), 064021 (2006).
124. R. Choe et al., "Optically measured microvascular blood flow contrast of malignant breast tumors," *PLoS One* **9**(6), e99683 (2014).
125. D. R. Busch et al., "Blood flow reduction in breast tissue due to mammographic compression," *Acad. Radiol.* **21**(2), 151–161 (2014).
126. S. Fantini et al., "Assessment of the size, position, and optical properties of breast tumors in vivo by noninvasive optical methods," *Appl. Opt.* **37**(10), 1982 (1998).
127. B. J. Tromberg et al., "Non-invasive *in vivo* characterization of breast tumors using photon migration spectroscopy," *Neoplasia* **2**(1–2), 26–40 (2000).
128. M. J. Holboke et al., "Three-dimensional diffuse optical mammography with ultrasound localization in a human subject," *J. Biomed. Opt.* **5**(2), 237–247 (2000).
129. B. W. Pogue et al., "Quantitative hemoglobin tomography with diffuse near-infrared spectroscopy: pilot results in the breast," *Radiology* **218**(1), 261–266 (2001).
130. Q. Zhu et al., "Early-stage invasive breast cancers: potential role of optical tomography with US localization in assisting diagnosis," *Radiology* **256**(2), 367–378 (2010).
131. D. Grosenick et al., "Time-domain scanning optical mammography: I. Recording and assessment of mammograms of 154 patients," *Phys. Med. Biol.* **50**(11), 2429–2449 (2005).
132. P. Taroni et al., "Time-resolved optical mammography between 637 and 985 nm: clinical study on the detection and identification of breast lesions," *Phys. Med. Biol.* **50**(11), 2469–2488 (2005).
133. Q. Zhu et al., "Benign versus malignant breast masses: optical differentiation with US-guided optical imaging reconstruction," *Radiology* **237**(1), 57–66 (2005).
134. D. Grosenick et al., "Time-domain scanning optical mammography: II. Optical properties and tissue parameters of 87 carcinomas," *Phys. Med. Biol.* **50**(11), 2451–2468 (2005).
135. L. Spinelli et al., "Characterization of female breast lesions from multi-wavelength time-resolved optical mammography," *Phys. Med. Biol.* **50**(11), 2489–2502 (2005).
136. S. P. Poplack et al., "Electromagnetic breast imaging: results of a pilot study in women with abnormal mammograms," *Radiology* **243**(2), 350–359 (2007).
137. G. Quarto et al., "Optical discrimination between malignant and benign breast lesions," *Proc. SPIE* **9538**, 953814 (2015).
138. H. Rinneberg et al., "Scanning time-domain optical mammography: detection and characterization of breast tumors *in vivo*," *Technol. Cancer Res. Treat.* **4**(5), 483–496 (2005).
139. D. A. Boas and M. A. Franceschini, "Haemoglobin oxygen saturation as a biomarker: the problem and a solution," *Philos. Trans. A: Math. Phys. Eng. Sci.* **369**(1955), 4407–4424 (2011).
140. S. H. Chung et al., "Macroscopic optical physiological parameters correlate with microscopic proliferation and vessel area breast cancer signatures," *Breast Cancer Res.* **17**(1), 72 (2015).
141. M. G. Pakalniskis et al., "Tumor angiogenesis change estimated by using diffuse optical spectroscopic tomography: demonstrated correlation in women undergoing neoadjuvant chemotherapy for invasive breast cancer?," *Radiology* **259**(2), 365–374 (2011).

142. C. Li et al., "Noninvasive *in vivo* tomographic optical imaging of cellular morphology in the breast: Possible convergence of microscopic pathology and macroscopic radiology," *Med. Phys.* **35**(6), 2493–2501 (2008).
143. P. Taroni et al., "Absorption of collagen: effects on the estimate of breast composition and related diagnostic implications," *J. Biomed. Opt.* **12**(1), 014021 (2007).
144. X. Gu et al., "Differentiation of cysts from solid tumors in the breast with diffuse optical tomography," *Acad. Radiol.* **11**(1), 53–60 (2004).
145. Y. Zhao et al., "Optimization of image reconstruction for magnetic resonance imaging-guided near-infrared diffuse optical spectroscopy in breast," *J. Biomed. Opt.* **20**(5), 056009 (2015).
146. M. A. Mastanduno et al., "MR-guided near-infrared spectral tomography increases diagnostic performance of breast MRI," *Clin. Cancer Res.* **21**(17), 3906–3912 (2015).
147. S. Kukreti et al., "Characterization of metabolic differences between benign and malignant tumors: high-spectral-resolution diffuse optical spectroscopy," *Radiology* **254**(1), 277–284 (2010).
148. S. Fantini et al., "Spatial and spectral information in optical mammography," *Technol. Cancer Res. Treat.* **4**(5), 471–482 (2005).
149. M. L. Flexman et al., "Digital optical tomography system for dynamic breast imaging," *J. Biomed. Opt.* **16**(7), 076014 (2011).
150. L. S. Fournier et al., "Dynamic optical breast imaging: a novel technique to detect and characterize tumor vessels," *Eur. J. Radiol.* **69**(1), 43–49 (2009).
151. M. D'Aiuto et al., "The dynamic optical breast imaging in the preoperative workflow of women with suspicious or malignant breast lesions: development of a new comprehensive score," *ISRN Oncol.* **2012**, 631917 (2012).
152. V. Frattini et al., "Clinical approach with optical imaging instrument. Perspective analysis on 617 young females," *It. J. Gynaecol. Obstet.* **23**(2/3), 101–106 (2011).
153. R. X. Xu et al., "A prospective pilot clinical trial evaluating the utility of a dynamic near-infrared imaging device for characterizing suspicious breast lesions," *Breast Cancer Res.* **9**(6), R88 (2007).
154. C. M. Carpenter et al., "Inspired gas-induced vascular change in tumors with magnetic-resonance-guided near-infrared imaging: human breast pilot study," *J. Biomed. Opt.* **15**(3), 036026 (2010).
155. .S. S. Dixit et al., "Near infrared transillumination imaging of breast cancer with vasoactive inhalation contrast," *Biomed. Opt. Express* **1**(1), 295–309 (2010).
156. C. M. Carpenter et al., "Monitoring of hemodynamic changes induced in the healthy breast through inspired gas stimuli with MR-guided diffuse optical imaging," *Med. Phys.* **37**(4), 1638–1646 (2010).
157. S. Jiang et al., "In vivo near-infrared spectral detection of pressure-induced changes in breast tissue," *Opt. Lett.* **28**(14), 1212–1214 (2003).
158. S. Jiang et al., "Measurement of pressure-displacement kinetics of hemoglobin in normal breast tissue with near-infrared spectral imaging," *Appl. Opt.* **48**(10), D130–D136 (2009).
159. S. A. Carp et al., "Compression-induced changes in the physiological state of the breast as observed through frequency domain photon migration measurements," *J. Biomed. Opt.* **11**(6), 064016 (2006).
160. S. A. Carp et al., "Dynamic functional and mechanical response of breast tissue to compression," *Opt. Express* **16**(20), 16064–16078 (2008).
161. X. Intes et al., "*In vivo* continuous-wave optical breast imaging enhanced with indocyanine green," *Med. Phys.* **30**(6), 1039 (2003).
162. A. Hagen et al., "Late-fluorescence mammography assesses tumor capillary permeability and differentiates malignant from benign lesions," *Opt. Express* **17**(19), 17016 (2009).
163. A. Poellinger et al., "Breast cancer: early-and late-fluorescence near-infrared imaging with indocyanine green—a preliminary study," *Radiology* **258**(2), 409–416 (2011).
164. C. Perlitz et al., "Comparison of two tricarbocyanine-based dyes for fluorescence optical imaging," *J. Fluoresc.* **15**(3), 443–454 (2005).
165. A. Poellinger et al., "Near-infrared imaging of the breast using omocianine as a fluorescent dye: results of a placebo-controlled, clinical, multicenter trial," *Invest. Radiol.* **46**(11), 697–704 (2011).
166. S. P. Gampenrieder, G. Rinnerthaler, and R. Greil, "Neoadjuvant chemotherapy and targeted therapy in breast cancer: past, present, and future," *J. Oncol.* **2013**, 732047 (2013).
167. P. Rastogi et al., "Preoperative chemotherapy: updates of national surgical adjuvant breast and bowel project protocols B-18 and B-27," *J. Clin. Oncol.* **26**(5), 778–785 (2008).
168. D. Roblyer et al., "Optical imaging of breast cancer oxyhemoglobin flare correlates with neoadjuvant chemotherapy response one day after starting treatment," *Proc. Natl. Acad. Sci. U. S. A.* **108**(35), 14626–14631 (2011).
169. D. B. Jakubowski et al., "Monitoring neoadjuvant chemotherapy in breast cancer using quantitative diffuse optical spectroscopy: a case study," *J. Biomed. Opt.* **9**(1), 230–238 (2004).
170. A. E. Cerussi et al., "Predicting response to breast cancer neoadjuvant chemotherapy using diffuse optical spectroscopy," *Proc. Natl. Acad. Sci. U. S. A.* **104**(10), 4014–4019 (2007).
171. S. Ueda et al., "Baseline tumor oxygen saturation correlates with a pathologic complete response in breast cancer patients undergoing neoadjuvant chemotherapy," *Cancer Res.* **72**(17), 4318–4328 (2012).
172. H. Soliman et al., "Functional imaging using diffuse optical spectroscopy of neoadjuvant chemotherapy response in women with locally advanced breast cancer," *Clin. Cancer Res.* **16**(9), 2605–2614 (2010).
173. O. Falou et al., "Diffuse optical spectroscopy evaluation of treatment response in women with locally advanced breast cancer receiving neoadjuvant chemotherapy," *Transl. Oncol.* **5**(4), 238–246 (2012).
174. Q. Zhu et al., "Breast cancer: assessing response to neoadjuvant chemotherapy by using US-guided near-infrared tomography," *Radiology* **266**(2), 433–442 (2013).
175. Q. Zhu et al., "Pathologic response prediction to neoadjuvant chemotherapy utilizing pretreatment near-infrared imaging parameters and tumor pathologic criteria," *Breast Cancer Res.* **16**(5), 456 (2014).
176. S. Jiang et al., "Predicting breast tumor response to neoadjuvant chemotherapy with diffuse optical spectroscopic tomography prior to treatment," *Clin. Cancer Res.* **20**(23), 6006–6015 (2014).
177. S. Jiang et al., "Evaluation of breast tumor response to neoadjuvant chemotherapy with tomographic diffuse optical spectroscopy: case studies of tumor region-of-interest changes," *Radiology* **252**(2), 551–560 (2009).
178. C. Zhou et al., "Diffuse optical monitoring of blood flow and oxygenation in human breast cancer during early stages of neoadjuvant chemotherapy," *J. Biomed. Opt.* **12**(5), 051903 (2007).
179. J. Gunther et al., "Combined dynamic and static optical tomography for prediction of treatment outcome in breast cancer patients," *Proc. SPIE* **9538**, 953811 (2015).
180. R. Choe et al., "Diffuse optical tomography of breast cancer during neoadjuvant chemotherapy: a case study with comparison to MRI," *Med. Phys.* **32**(4), 1128–1139 (2005).
181. L. C. Enfield et al., "Monitoring the response to primary medical therapy for breast cancer using three- dimensional time-resolved optical mammography," *Technol. Cancer Res. Treat.* **10**(6), 533–547 (2011).
182. B. E. Schaafsma et al., "Optical mammography using diffuse optical spectroscopy for monitoring tumor response to neoadjuvant chemotherapy in women with locally advanced breast cancer," *Clin. Cancer Res.* **21**(3), 577–584 (2015).
183. B. J. Tromberg et al., "OT2-05-02: ACRIN 6691 monitoring and predicting breast cancer neoadjuvant chemotherapy response using diffuse optical spectroscopic imaging (DOSI)," *Cancer Res.* **71**(24 Suppl.), OT2-OT05– 02 (2011).
184. E. A. Sickles et al., "ACR BI-RADS® mammography," in *ACR BI-RADS® Atlas, Breast Imaging Reporting and Data System*, American College of Radiology, Reston Virginia (2013).
185. V. A. McCormack and S. Silva, "Breast density and parenchymal patterns as markers of breast cancer risk: a meta-analysis," *Cancer Epidemiol. Biomarkers Prev.* **15**, 1159–1169 (2006).
186. T. Cil et al., "Mammographic density and the risk of breast cancer recurrence after breast-conserving surgery," *Cancer* **115**(24), 5780–5787 (2009).
187. N. F. Boyd et al., "Mammographic density and breast cancer risk: current understanding and future prospects," *Breast Cancer Res.* **13**(6), 223 (2011).
188. US Preventive Services Task Force, "Chemoprevention of breast cancer: recommendations and rationale," *Ann. Intern. Med.* **137**(1), 56 (2002).

189. S. Elsamany et al., "Mammographic breast density: predictive value for pathological response to neoadjuvant chemotherapy in breast cancer patients," *Breast* **24**(5), 576–581 (2015).
190. J. Kim et al., "Breast density change as a predictive surrogate for response to adjuvant endocrine therapy in hormone receptor positive breast cancer," *Breast Cancer Res.* **14**(4), R102 (2012).
191. J. Bastos et al., "The state of the art of cancer control in 30 European countries in 2008," *Int. J. Cancer* **126**(11), 2700–2715 (2010).
192. N. Boyd et al., "Breast-tissue composition and other risk factors for breast cancer in young women: a cross-sectional study," *Lancet Oncol.* **10**(6), 569–580 (2009).
193. N. A. Lee et al., "Fatty and fibroglandular tissue volumes in the breasts of women 20–83 years old: comparison of X-ray mammography and computer-assisted MR imaging," *Am. J. Roentgenol.* **168**(2), 501–506 (1997).
194. K. M. Blackmore, J. A. Knight, and L. Lilge, "Association between transillumination breast spectroscopy and quantitative mammographic features of the breast," *Cancer Epidemiol. Biomarkers Prev.* **17**(5), 1043–1050 (2008).
195. J. W. Byng et al., "Automated analysis of mammographic densities and breast carcinoma risk," *Cancer* **80**(1), 66–74 (1997).
196. P. Taroni et al., "Noninvasive assessment of breast cancer risk using time-resolved diffuse optical spectroscopy," *J. Biomed. Opt.* **15**(6), 060501 (2010).
197. S. Srinivasan et al., "Interpreting hemoglobin and water concentration, oxygen saturation, and scattering measured *in vivo* by near-infrared breast tomography," *Proc. Natl. Acad. Sci. U. S. A.* **100**(21), 12349–12354 (2003).
198. X. Wang et al., "Approximation of Mie scattering parameters in near-infrared tomography of normal breast tissue *in vivo*," *J. Biomed. Opt.* **10**(5), 051704 (2005).
199. N. Shah et al., "The role of diffuse optical spectroscopy in the clinical management of breast cancer," *Dis. Markers* **19**(2–3), 95–105 (2004).
200. C. Luparello, "Aspects of collagen changes in breast cancer," *J. Carcinog. Mutagen.* **S13**, 7 (2013).
201. Y.-P. Guo et al., "Growth factors and stromal matrix proteins associated with mammographic densities," *Cancer Epidemiol. Biomarkers Prev.* **10**, 243–248 (2001).
202. P. P. Provenzano et al., "Collagen reorganization at the tumor-stromal interface facilitates local invasion," *BMC Med.* **4**(1), 38 (2006).
203. A. Pifferi et al., "Collagen content as a risk factor in breast cancer? a pilot clinical study," *Proc. SPIE* **9538**, 953813 (2015).
204. P. Taroni et al., "Breast tissue composition and its dependence on demographic risk factors for breast cancer: non-invasive assessment by time domain diffuse optical spectroscopy," *PLoS One* **10**(6), e0128941 (2015).
205. A. A. Oraevsky et al., "Breast cancer diagnostics by laser optoacoustic tomography," in *Trends Opt. Photonics*, R. R. Alfano and J. G. Fujimoto, Eds., pp. 316–321, OSA Publishing House, Washington, D.C. (1996).
206. J. Menke, "Photoacoustic breast tomography prototypes with reported human applications," *Eur. Radiol.* **25**(8), 2205–2213 (2015).
207. M. Heijblom et al., "Photoacoustic image patterns of breast carcinoma and comparisons with magnetic resonance imaging and vascular stained histopathology," *Sci. Rep.* **5**, 11778 (2015).
208. M. Heijblom et al., "Appearance of breast cysts in planar geometry photoacoustic mammography using 1064-nm excitation," *J. Biomed. Opt.* **18**(12), 126009 (2013).
209. M. Heijblom et al., "Visualizing breast cancer using the Twente photoacoustic mammoscope: what do we learn from twelve new patient measurements?," *Opt. Express* **20**(11), 11582–11597 (2012).
210. S. Manohar et al., "Initial results of *in vivo* non-invasive cancer imaging in the human breast using near-infrared photoacoustics," *Opt. Express* **15**(19), 12277–12285 (2007).
211. K. Fukutani et al., "Characterization of photoacoustic tomography system with dual illumination," *Proc. SPIE* **7899**, 78992J (2011).
212. A. A. Oraevsky et al., "Laser optoacoustic imaging of breast cancer *in vivo*," *Proc. SPIE* **4256**, 6–15 (2001).
213. S. A. Ermilov et al., "Laser optoacoustic imaging system for detection of breast cancer," *J. Biomed. Opt.* **14**(2), 024007 (2009).
214. R. A. Kruger et al., "Dedicated 3D photoacoustic breast imaging," *Med. Phys.* **40**(11), 113301 (2013).
215. C. Haisch et al., "Combined optoacoustic/ultrasound system for tomographic absorption measurements: possibilities and limitations," *Anal. Bioanal. Chem.* **397**(4), 1503–1510 (2010).
216. C. Kim et al., "Deeply penetrating *in vivo* photoacoustic imaging using a clinical ultrasound array system," *Biomed. Opt. Express* **1**(1), 278–284 (2010).
217. Z. Xie et al., "Combined photoacoustic and acoustic imaging of human breast specimens in the mammographic geometry," *Ultrasound Med. Biol.* **39**(11), 2176–2184 (2013).
218. X. L. Deán-Ben and D. Razansky, "Portable spherical array probe for volumetric real-time optoacoustic imaging at centimeter-scale depths," *Opt. Express* **21**(23), 28062–28071 (2013).
219. X. L. Deán-Ben and D. Razansky, "Functional optoacoustic human angiography with handheld video rate three dimensional scanner," *Photoacoustics* **1**(3–4), 68–73 (2013).
220. K. Daoudi et al., "Handheld probe integrating laser diode and ultrasound transducer array for ultrasound/photoacoustic dual modality imaging," *Opt. Express* **22**(21), 26365–26374 (2014).
221. A. A. Oraevsky, "'Contrast agents for optoacoustic imaging: design and biomedical applications'," *Photoacoustics* **3**(1), 1–2 (2015).
222. L. A. Sordillo et al., "Deep optical imaging of tissue using the second and third near-infrared spectral windows," *J. Biomed. Opt.* **19**(5), 056004 (2014).
223. R. Nachabé et al., "Estimation of biological chromophores using diffuse optical spectroscopy: benefit of extending the UV-VIS wavelength range to include 1000 to 1600 nm," *Biomed. Opt. Express* **1**(5), 1432–1442 (2010).
224. S. Konugolu Venkata Sekar et al., "Broadband (600–1350 nm) time resolved diffuse optical spectrometer for clinical use," *IEEE J. Sel. Top. Quantum Electron.* **22**(3), 406–414 (2016).
225. P. Tracqui, "Biophysical models of tumour growth," *Reports Prog. Phys.* **72**(5), 056701 (2009).
226. H. Rieger and M. Welter, "Integrative models of vascular remodeling during tumor growth," *Wiley Interdiscip. Rev. Syst. Biol. Med.* **7**(3), 113–129 (2015).

Dirk Grosenick is head of the Optical Medical Imaging Working Group at Physikalisch-Technische Bundesanstalt (PTB) Berlin. He received his PhD in physics on femtosecond laser spectroscopy and nonlinear optics. His research interests are in the fields of near-infrared spectroscopy and functional imaging of biological tissue, in the determination of healthy and diseased tissue optical properties, and in contrast-enhanced fluorescence imaging for diagnostics and therapy of diseases.

Herbert Rinneberg received his PhD in physical chemistry from the University of Frankfurt, Germany in 1968. After his habilitation in experimental physics at the Free University of Berlin (FUB) in 1980 he was appointed adjunct professor of physics at FUB in 1988. In 1987 he joined Physikalisch-Technische Bundesanstalt (PTB) Berlin, establishing research in biomedical optics, including optical mammography, and in high-field MRI for medical applications. He served as head of the division of medical physics and metrological information technology until his retirement in 2004. His research interests covered nuclear solid state physics, atomic physics and medical physics.

Rinaldo Cubeddu started his academic career at the Physics Department of Politecnico di Milano, where he became full professor in physics on 1987. Following his retirement in 2014, he was appointed Professor Emeritus. His research activity is mostly located in biophotonics where he pioneered the use of time-domain instrumentation. Beside fundamental research he developed clinical instrumentation as a FLIM system, an optical mammograph and a pulsed oximeter.

Paola Taroni is full professor of physics at Politecnico di Milano in Milan, Italy since 2011. She is coauthor of more than 120 scientific papers in international peer-reviewed journals. Her research activity concerns mainly the development of photonics systems for time-resolved spectroscopy and imaging, and their diagnostic applications in biology and medicine, including time domain diffuse optical spectroscopy, with special attention to breast imaging and spectroscopy, and time-resolved fluorescence spectroscopy and fluorescence lifetime imaging for medical diagnostics and microscopy.